Applied and Environmental Microbiology

Osmotic stress response of the coral and oyster pathogen *Vibrio coralliilyticus*: acquisition of catabolism gene clusters for the compatible solute and signaling molecule *myo*-inositol

Katherine E. Boas Lichty[1], Rachel M. Loughran[2], Blake Ushijima[3], Gary P. Richards[4], and E. Fidelma Boyd*[1]

[1]Department of Biological Sciences, University of Delaware, Newark, DE19716

[2]Microbiology Graduate Program, University of Delaware, Newark, DE, USA

[3]Department of Biology and Marine Biology, University of North Carolina Wilmington, Wilmington, NC, USA

[4]U.S. Department of Agriculture, Agricultural Research Service, Dover, Delaware, USA

Corresponding author*

Prof. E. Fidelma Boyd

Department of Biological Sciences

341 Wolf Hall, University of Delaware
Newark, DE 19716

Phone: (302) 831-1088. Fax: (302) 831-2281 Email: fboyd@udel.edu

Running title: marine bacteria acquire myo-inositol catabolism clusters

Key words: myo-inositol compatible solutes nutrient.

ABSTRACT Marine bacteria experience fluctuations in osmolarity that they must adapt to, and most bacteria respond to high osmolarity by accumulating compatible solutes also known as osmolytes. The osmotic stress response and compatible solutes used by the coral and oyster pathogen *Vibrio coralliilyticus* were unknown. In this study, we showed that to alleviate osmotic stress *V. coralliilyticus* biosynthesized glycine betaine (GB) and transported into the cell choline, GB, ectoine, dimethylglycine, and dimethylsulfoniopropionate, but not *myo*-inositol. *Myo*-inositol is a stress protectant and a signaling molecule that is biosynthesized and used by algae. Bioinformatics identified *myo*-inositol (*iol*) catabolism clusters in *V. coralliilyticus* and other *Vibrio*, *Photobacterium*, *Grimontia*, and *Enterovibrio* species. Growth pattern analysis demonstrated that *V. coralliilyticus* utilized *myo*-inositol as a sole carbon source, with a short lag time of 3 h. An *iolG* deletion mutant, which encodes an inositol dehydrogenase, was unable to grow on *myo*-inositol. Within the *iol* clusters were an MFS-type (*iolT1*) and an ABC-type (*iolXYZ*) transporter and analyses showed that both transported *myo*-inositol. IolG and IolA phylogeny among *Vibrionaceae* species showed different evolutionary histories indicating multiple acquisition events. Outside of *Vibrionaceae*, IolG was most closely related to IolG from a small group of *Aeromonas* fish and human pathogens and *Providencia* species. However, IolG from hypervirulent *A. hydrophila* strains clustered with IolG from *Enterobacter*, and divergently from *Pectobacterium*, *Brenneria*, and *Dickeya* plant pathogens. The *iol* cluster was also present within *Aliiroseovarius*, *Burkholderia*, *Endozoicomonas*, *Halomonas*, *Labrenzia*, *Marinomonas*, *Marinobacterium*, *Cobetia*, *Pantoea*, and *Pseudomonas*, of which many species were associated with marine flora and fauna.

IMPORTANCE Host associated bacteria such as *V. coralliilyticus* encounter competition for nutrients and have evolved metabolic strategies to better compete for food. Emerging studies show that *myo*-inositol is exchanged in the coral-algae symbiosis, is likely involved in signaling, but is also an osmolyte in algae. The bacterial consumption

of *myo*-inositol could contribute to a breakdown of the coral-algae symbiosis during thermal stress or disrupt the coral microbiome. Phylogenetic analyses showed that the evolutionary history of *myo*-inositol metabolism is complex, acquired multiple times in *Vibrio*, but acquired once in many bacterial plant pathogens. Further analysis also showed that a conserved *iol* cluster is prevalent among many marine species (commensals, mutualists, and pathogens) associated with marine flora and fauna, algae, sponges, corals, molluscs, crustaceans, and fish.

58 **INTRODUCTION**

59 *Vibrio coralliilyticus* is a marine bacterium, a member of the family *Vibrionaceae*, an
60 important pathogen of coral, and along with *V. mediterranei* (previously *V. shilonii*) a
61 source of coral disease worldwide (1-10). This species was first characterized as an
62 etiological agent for coral bleaching and tissue loss of the coral *Pocillopora damicornis*,
63 and has since been identified as a pathogen in numerous other species of coral (2, 3, 6,
64 11-23). Recent studies also showed that *V. coralliilyticus* and a related species *V. tubiashii*
65 caused high mortalities in oyster larvae of both Pacific oysters (*Crassostrea gigas*) and
66 Eastern oysters (*Crassostrea virginica*) in the United States (15, 24-29).

67 Vibriosis in corals as well as oyster larvae is linked to increased water
68 temperatures, especially for select strains of the pathogen *V. coralliilyticus* (2, 23, 25). In
69 response to elevated temperatures, *V. coralliilyticus* undergoes various changes to its
70 transcriptome and proteome (11, 13), which includes various genes important for
71 infections of hosts like corals (23). The increased temperatures also correlates with the
72 increased abundance of *V. coralliilyticus* (5), and the structure of natural *Vibrio*
73 populations could be altered within the coral holobiont (30-32). This restructuring is
74 proposed to contribute to disruption of processes like the nutritional exchange within
75 the coral (33) as well as the healthy coral microbiome (34, 35). One consequence of
76 infection is bleaching, the loss of the corals' endosymbiotic dinoflagellates (family
77 *Symbiodiniaceae*), that occurs with select pathogenic strains of *V. coralliilyticus* (2, 17). The
78 photosynthetic dinoflagellate cells participate in a nutrient exchange with the host coral
79 cells, which serves as the main energy source for many reef-building coral species (36-
80 41). This metabolic exchange with photosynthetic dinoflagellates is central to
81 maintaining the health of this mutualistic relationship (42-47).

82 One metabolite exchanged between dinoflagellates and coral is the carbocyclic
83 sugar *myo*-inositol hypothesized to be transported to coral with a function not yet

84 established (37, 38, 48). *Myo*-inositol is a six-carbon cyclic polyol and the most abundant
85 form of inositol in the environment. It is an important component of eukaryotic cell
86 membranes as phosphatidylinositol (PI) and a signaling molecule (49-51). In
87 dinoflagellates inositol isomers are biosynthesized as important compatible solutes and
88 are significantly enriched during thermal stress (38, 48, 52-55). In response to increased
89 salinity, algae, plants, and marine invertebrates use *myo*-inositol as a compatible solute
90 for osmotic stress protection (56-58). Additionally, in algae and plants, *myo*-inositol has
91 been implicated as an important signaling molecule (48, 54, 55, 59).

92 Studies have shown that soil bacteria and human bacterial pathogens can utilize
93 inositols as carbon and energy sources (60, 61). The first step in the pathway requires
94 inositol dehydrogenases (IDHs), which are specific for different isomers of inositol such
95 as *myo*-, *scyllo*-, and d-*chiro*-inositol. Genetics and enzyme functionality studies for
96 bacterial *myo*-inositol catabolism genes were first established and investigated in
97 *Bacillus subtilis* (62-65) (**Fig. 1**). *Myo*-inositol is degraded by inositol 2-dehydrogenase
98 (IolG) into 2-keto-*myo*-inositol, which is then converted by *myo*-inosose dehydratase
99 (IolE) to 3,5/4-Trihydroxycylohexane-1,2-dione. This is subsequently hydrolyzed into 5-
100 deoxy-D-gluconate by an acylhydrolase (IolD). This product is then isomerized by 5-
101 deoxy-glucuronate isomerase (IolB) and phosphorylated by 5-dehydro-2-
102 deoxygluconokinase (IolC). Then 2-deoxy-5-keto-D-gluconate-6-P is converted to
103 dihydroxyacetone (DHA) and malonate semialdehyde by an aldolase (IolJ). Malonate
104 semialdehyde is converted to acetyl-CoA by the CoA-acylating methylmalonate-
105 semialdehyde dehydrogenase (IolA). The product DHA can enter glycolysis and acetyl-
106 CoA can enter the tricarboxylic acid (TCA) cycle (63-66). The transport of *myo*-inositol
107 into *B. subtilis* for catabolism is performed by two major facilitator superfamily (MFS)-
108 type transporters, named IolT and IolF (63). Several Gram-negative bacteria have been
109 shown to use *myo*-inositol as a metabolite with a similar pathway, species in the genera

110 *Klebsiella, Caulobacter, Rhizobium, Sinorhizobium, Pseudomonas, Yersinia, Corynebacterium,*
111 *Salmonella*, and *Serratia* (67-76). For example, the human pathogen *Salmonella enterica*
112 serovar Typhimurium utilized *myo*-inositol as a sole carbon source, but growth on *myo*-
113 inositol was characterized by a long lag phase of > 45 h and a bistable phenotype (61, 69,
114 70, 77, 78). This species uses two MFS family transporters, named IolT1 and IolT2 for
115 *myo*-inositol uptake (70). In the Alpha-proteobacteria *Caulobacter vibrioides* (formerly
116 *crescentus*) catabolism of *myo*-inositol was demonstrated and an ABC-type transporter
117 was used for uptake (68, 79). *Myo*-inositol utilization has not been explored extensively
118 among other marine bacteria.

119 Here, we established osmotic stress response mechanisms using bioinformatics
120 and genetic analyses among *V. coralliilyticus* strains CN52H-1 (16), OCN014 (23), BAA-
121 450 (19), and RE87 (80, 81) encompassing strains isolated from healthy and diseased
122 hosts. We examined *V. coralliilyticus* growth patterns at different temperatures and
123 salinities to determine their salinity tolerance. Bioinformatics and physiological
124 approaches were employed to determine the compatible solutes used by of *V.*
125 *coralliilyticus* for osmotic protection. Our investigations led to the identification of a
126 large genomic region containing genes for *myo*-inositol catabolism, a molecule used in
127 many eukaryotic cellular functions including stress protection and signaling. Using
128 comparative genomics and phylogenetic analyses, the evolutionary history of *myo*-
129 inositol catabolism genes among the *Vibrionaceae* was established. The distribution of *iol*
130 clusters among marine bacteria was also examined.

131 **RESULTS**

132 ***Vibrio coralliilyticus* salinity and temperature range.** To determine the ability of *V.*
133 *coralliilyticus* to grow in a range of NaCl concentrations and at different temperatures,
134 growth patterns were examined in M9 minimal media supplemented with 20 mM
135 glucose (M9G) and a final concentration of 1% to 6% NaCl at 28°C and 37°C for 24 h.

136 M9 minimal media was used for growth assays because it does not contain compatible
137 solutes or their precursors and this allowed us to examine the response of *V.*
138 *coralliilyticus* to increased salinity without the protection of external compatible solutes.
139 These analyses showed that the *V. coralliilyticus* strains grew best in M9G 2% NaCl at
140 28°C (**Fig. 2**). For example, at this temperature, for strain CN52H-1, the final OD_{595}
141 reading was 0.81 in 2% NaCl whereas in 1% NaCl, the final OD reached was 0.49. When
142 the salinity was increased to 3% NaCl the maximum growth rate (0.62 h^{-1}) was lower
143 than what was observed at 2% NaCl (0.70 h^{-1}). Growth of *V. coralliilyticus* in 4% NaCl
144 showed a 2 h lag time and a lower maximum growth rate (0.33 h^{-1}) whereas no growth
145 occurred in 5% and 6% NaCl (**Fig. 2A**). Next, we tested whether increased temperature
146 affected the salinity growth range by examining growth at 37°C (**Fig. 2B**). Interestingly,
147 incubation at 37°C impacted the ability to grow in low salinity; at this temperature there
148 was no growth in 1% NaCl (**Fig. 2B**). Growth pattern analysis was also performed on *V.*
149 *coralliilyticus* OCN014 (**Fig. 2C-D**), BAA-450 (**Fig. 2E-F**), and RE87 (**Fig. 2G-H**),
150 pathogenic strains of corals and oyster larvae in 1% to 6% NaCl at 28°C and 37°C for 24
151 h. We also examined the salinity growth range at 21°C and 34°C for strain CN52H-1
152 (**Fig. S1A-B**). Two observations were made from these analyses; first incubation at 21°C
153 negatively affected growth in 4% NaCl resulting in a longer lag phase than at any other
154 temperature (**Fig. S1B**). Secondly, growth at 34°C was similar to 28°C, but with a longer
155 lag phase in M9G 4% NaCl (**Fig. S1A**). These analyses demonstrated that *V.*
156 *coralliilyticus* was unable to grow in M9G media with a salinity at or above 5% NaCl and
157 at 37°C strains were unable to grow in 1% NaCl (**Fig. 2**). Overall, all strains showed
158 similar osmotic stress tolerance responses.

159 ***V. coralliilyticus* biosynthesizes glycine betaine (GB) and uptakes numerous**
160 **compatible solutes for osmotic protection.** Bioinformatics analysis of *V. coralliilyticus*
161 genomes identified the *betIBA* cluster encoding homologs of enzymes required for the

162 biosynthesis of GB from choline and six putative compatible solute transporters in all 35
163 strains present in the NCBI genome database (as of March 2024). To confirm
164 biosynthesis of GB from choline, ^{1}H-nuclear magnetic resonance analysis (^{1}H-NMR) was
165 performed with *V. coralliilyticus* cells grown in M9G 4% NaCl with 1 mM choline and
166 from cells grown in the absence of choline. ^{1}H-NMR spectral analysis of ethanol extracts
167 did not show any peaks in the absence of choline, but GB peaks were present in
168 CN52H-1 cells (**Fig. 3A-B**) grown in M9G 4% NaCl supplemented with choline and in
169 strains OCN014 (**Fig. S2**) and BAA-450 (data not shown). To determine the compatible
170 solutes that are transported into the cell for osmotic stress protection, the growth of *V.*
171 *coralliilyticus* strain CN52H-1 was examined in M9G 5% NaCl supplemented with one of
172 ten different compatible solutes (**Fig. 3C, Fig. S3**). In the absence of compatible solutes
173 in the media, *V. coralliilyticus* does not grow in M9G 5% NaCl as demonstrated (**Fig. 2,**
174 **Fig. S3**). The growth pattern of *V. coralliilyticus* cells grown in each compatible solute
175 was monitored for 24 h at 28°C and area under the curve (AUC) was calculated (**Fig.**
176 **3C**). Seven of the ten compatible solutes tested allowed growth in M9G 5% NaCl,
177 suggesting they were taken up and used for osmotic stress protection (**Fig. 3C**). The
178 presence of trimethylamine-N-oxide, *myo*-inositol (MI), or glycerol did not allow
179 growth in M9G 5% NaCl (**Fig. S3**). GB, dimethylsulfoniopropionate (DMSP), ectoine,
180 choline, or dimethylglycine (DMG) rescued growth to the greatest extent reaching a
181 final OD_{595} ranging from 0.45 to 0.69 (**Fig. S3**). The compatible solutes γ-amino-butyric
182 acid (GABA) and creatine had longer lag phase times with lower final OD_{595} of 0.23 and
183 0.31, respectively indicating that they were less effective as osmolytes (**Fig. S3**).

184 ***Myo*-inositol catabolism clusters are present in all strains of *V. coralliilyticus* and *V.***
185 ***mediterranei*.** Bioinformatics analysis identified putative *myo*-inositol catabolic gene
186 clusters that were present in all but one of the 35 *V. coralliilyticus* and 18 *V. mediterranei*,
187 a species also linked to coral disease, annotated genomes in the NCBI genome database

188 (as of March 2024). However, *V. coralliilyticus* SCSIO 43001 (82) was the sole exception,
189 the average nucleotide identify (ANI) of this strain with BAA-450 is only 87.85 which
190 suggests a misclassification of this strain. Therefore, strain SCSIO 43001 was not
191 included in this study. In *V. coralliilyticus* two distinct gene clusters for the regulation,
192 transport, and catabolism of *myo*-inositol were present (**Fig. 4A**), which we named
193 region 1 and 2. Gene annotation and naming were established based upon amino acid
194 similarity to the *myo*-inositol genes present in *Salmonella enterica.* No synteny was found
195 between *myo*-inositol gene clusters in *V. coralliilyticus* and *S. enterica* or *C. vibrioides* (**Fig.**
196 **S4**). Functionally similar genes were present in both region 1 and 2, but shared low
197 sequence similarity (27% to 50%) and lacked gene synteny between each other.

198 Region 1 contained fifteen genes, which included a predicted operon composed
199 of ten genes *iolEDidhiolCBJRIBG* encoding putative enzymes responsible for *myo*-
200 inositol conversion to dihydroxyacetone and malonate semialdehyde (**Fig. 4A and Fig.**
201 **1)**. Gene designations were based on sequence similarity to the *myo*-inositol cluster in *S.*
202 *enterica* (**Table S1**). Two copies of IolE and IolD are present, a copy in each region. The
203 *iolE* and *iolD* genes encode enzymes involved in the second and third steps of the
204 catabolic pathway. Region 1 copies are named IolE2 and IolD2 and shared 38% amino
205 acid identity to the enzymes from *S. enterica* (**Table S1**). The *iolC* gene encodes a
206 putative 5-dehydro-2-deoxyglucokinase and shared 33% amino acid identify with IolC
207 from *S. enterica*. The next step in the pathway is completed by an oxidoreductase
208 encoded by *iolB.* Two copies of this gene were found within region 1 (named *iolB*1 and
209 *iolB*2) that shared 63.5% and 31% amino acid identify respectively to IolB from *S.*
210 *enterica* (**Table S1**). The *iolG* gene encoded an inositol 2-dehydrogenase required for the
211 first step in the pathway. IolG shared 36.1% amino acid identity to IolG2 from *S.*
212 *enterica*. An *idh* gene within the operon encoded a Gfo/Idh/MocA-type oxidoreductase,
213 which could have a dehydrogenase function to convert isomers of inositol into the

214 degradation pathway. Region 1 also contained two MFS transporters, a LysR family
215 transcriptional regulator, a glycosyltransferase and a polysaccharide biosynthesis
216 protein.

217 Region 2 contained a predicted operon *iolCDEA*, which shared greater amino
218 acid identity with Iol in *S. enterica* than proteins in region 1, with similarity ranging
219 from 43.7% to 67.4% (**Table S1**). The *iolA* gene encoded a CoA-acylating
220 methylmalonate-semialdehyde dehydrogenase involved in the last step in the pathway
221 (**Fig. 4A**). Divergently transcribed from *iolCDEA* was *iolXYZR* that encoded an ABC-
222 type transporter IolXYZ and an RpiR-type regulator, which we named IolR1 as it shared
223 67% identity with IolR from *S. enterica* (**Fig. 4A**). *S. enterica* does not possess an ABC-
224 type transporter that uptakes *myo*-inositol, but the substrate binding protein IolX from
225 *V. coralliilyticus* shared 31% amino acid identity with IbpA a known transporter of *myo*-
226 inositol in *C. vibrioides* (79).

227 A similar gene arrangement in region 1 and 2 was present in the genomes *V.*
228 *coralliilyticus* strains CN52H-1, OCN014, BAA-450, and RE87 (**Fig. S5**). In *V. mediterranei*
229 (formerly *V. shilonii*), strains of which are also coral pathogens, a single *iol* cluster is
230 present comprised of 18 genes, putative operons *iolCA*, *iolXYZR*, *iolEDidhiolCBJRIBG*
231 and *iolT1lysR* (**Fig. S4)**. These data suggest that these strains have the potential to
232 catabolize *myo*-inositol as a sole carbon source. It is of interest to note, that species
233 belonging to the Harveyi clade, specifically 65 *V. harveyi*, 13 *V. campbellii*, 23 *V. owensii*,
234 and 10 *V. jasicida* strains in the NCBI genome database (as of March 2024), contained
235 *myo*-inositol region 1, but not region 2 (**Fig. S6**). That is, no *iolA* or *iolXYZ* homologs are
236 present in these species.

237 ***Vibrio coralliilyticus* can utilize *myo*-inositol as a sole carbon source.** To demonstrate
238 *myo*-inositol catabolism by *V. coralliilyticus* CN52H-1, OCN014, BAA-450, and RE87,
239 strains were grown in M9 2% NaCl media supplemented with 20 mM glucose or 20 mM

240 *myo*-inositol or no carbon source. In M9 2% NaCl supplemented with *myo*-inositol, *V.*
241 *coralliilyticus* CN52H-1 reached a final OD_{595} of 0.31 with a lag time of 3 h (**Fig. 4B**). In
242 M9 2% NaCl glucose, there was a 1 h lag phase and a final OD_{595} of 0.65 was recorded
243 and in the absence of a carbon source, no growth occurred (**Fig. 4B**). Next, we examined
244 the ability of strains OCN014, BAA-450, and RE87 to grow on *myo*-inositol as a sole
245 carbon source. As expected, these strains followed a similar pattern of growth as
246 CN52H-1 on *myo*-inositol or glucose as sole carbon sources (**Fig. 4C**). We then examined
247 a *V. harveyi* strain since it only contained region 1 to determine whether growth on *myo*-
248 inositol can still occur. *V. harveyi* grew in M9 2% NaCl glucose but did not grow in *myo*-
249 inositol as a sole carbon source, whereas the control *V. coralliilyticus* did (**Fig. 4D**). This
250 suggested that region 2 is essential for *myo*-inositol catabolism, likely requiring the *iolA*
251 gene and/or *iolXYZ*. To demonstrate the requirement for region 1 for *myo*-inositol
252 catabolism, an in-frame non-polar deletion of *V. coralliilyticus iolG* (HRJ43_RS06535) was
253 constructed. The *iolG* gene encodes an inositol dehydrogenase essential in the first step
254 of the *myo*-inositol pathway and the last gene in region 1 of the *iol* operon (**Fig. 1**). To
255 demonstrate there was no overall growth defect in the construction of the Δ*iolG* mutant,
256 the strain was grown in M9 2% NaCl glucose, which showed a growth pattern identical
257 to the wild type strain (**Fig. 4E**). As expected, the Δ*iolG* strain showed no growth in M9
258 2% NaCl *myo*-inositol as a sole carbon source, with the wild type strain used as a
259 positive control (**Fig. 4E**). Overall, the data showed that *V. coralliilyticus* has a
260 functioning *myo*-inositol pathway and both regions 1 and 2 are required for catabolism.

261 **Ligand modeling predicts *V. coralliilyticus* IolT1 and IolXYZ are *myo*-inositol**
262 **transporters**. Two major facilitator superfamily (MFS)-type transporters are present
263 within region 1 and one ABC-type transporter IolXYZ within region 2. Ligand modeling
264 was performed by comparison to known transporters of *myo*-inositol to predict which
265 of these are likely responsible for *myo*-inositol transport. The MFS transporter from *B.*

266 *subtilis* IolT (WP_003234027.1) and *S. enterica* IolT1 (NP_463279.1) were selected as these
267 transporters were previously shown to transport *myo*-inositol (63). The MFS protein
268 (WP_099607352.1) within the region 1 cluster shared 48.8% amino acid identity to that
269 of *S. enterica* IolT1, which we named IolT1. Whereas the MFS protein (WP_172853823.1)
270 outside of the cluster shared only 25% similarity to that of *S. enterica*, which we named
271 MFS. Docking of *myo*-inositol with *B. subtilis* IolT and *S. enterica* IolT1 predicted a mode
272 of interaction with seven and five putative binding residues, respectively, and favorable
273 binding free energy changes (ΔG) of -7.0 kcal/mol and -6.1 kcal/mol. *Myo*-inositol
274 docking with *V. coralliilyticus* IolT1 predicted a favorable ΔG of -6.2 kcal/mol and four
275 putative binding residues. MFS-type transporters are known to coordinate substrate
276 binding with transmembrane (TM) domains TM7 and TM10 (83). Alignment of *B.*
277 *subtilis* IolT, *S. enterica* IolT1, *V. coralliilyticus* IolT1 and *V. coralliilyticus* MFS was
278 performed, and TM domains were identified. Predicted binding residues found in the
279 three models are shown with blue (*V. coralliilyticus* IolT1), green (*S. enterica* IolT1), and
280 orange (*B. subtilis* IolT) arrows, which were absent from MFS (**Fig. S7)**. The two
281 glutamine (Q273, Q274) and asparagine (N279) in TM7 are found in all three modeled
282 sequences. In TM10 three of the four sequences also contained a conserved tryptophan
283 (W377) residue. All three models predicted a residue that aligns at Y368. Both *V.*
284 *coralliilyticus* IolT1 and *S. enterica* IolT1 contain a conserved tyrosine (Y) residue here,
285 but *B. subtilis* IolT contained glutamine (Q) (**Fig. S7)**. Taken together this similarity in
286 the binding pockets of these transporters suggested that *V. coralliilyticus* IolT1 is likely
287 able to transport *myo*-inositol.

288 The ABC-type transporter substrate binding protein IbpA from *C. vibrioides* had
289 previously been shown to bind *myo*-inositol (79) and IolX (WP_227495657.1) from *V.*
290 *coralliilyticus* has 87% coverage and 31% amino acid identity to IbpA. Ligand docking
291 analysis of *myo*-inositol with IbpA and IolX predicted favorable modes of action with

292 ΔG of -7.4 kcal/mol and -5.3 kcal/mol, respectively. Putative binding residues were
293 identified for each substrate binding protein and are presented in the amino acid
294 alignment (**Fig. S8**). The green arrows indicate IbpA predicted binding residues and
295 blue arrows indicate IolX predicted binding residues. Five aligned residues were
296 predicted to be important in both docking models: 63 aspartic acid (D)/ glutamine (Q),
297 141 aspartic acid (D)/ asparagine (N), 187 glutamine (Q)/ serine (S), 269 aspartic acid
298 (D), and 289 glutamine (Q) (**Fig. S8B**). Based upon the favorable docking model and
299 select conserved residues in the alignment with a known *myo*-inositol transporter,
300 IolXYZ is predicted to be capable of *myo*-inositol transport.

301 **The MFS transporter IolT1 and ABC-type transporter IolXYZ are responsible for**
302 ***myo*-inositol uptake for catabolism**. To evaluate the ability of IolT1 and IolXYZ to
303 transport *myo*-inositol, in-frame non-polar deletion mutants were generated in the *iolT1*
304 (HRJ43_RS06585) and *iolX (HRJ43_RS06670)* genes and a double deletion mutant
305 *iolT1/iolX* was also constructed. To show that these mutants contained no overall
306 growth defects, all three mutants and wild type were each grown in M9 2% NaCl
307 supplemented with 20 mM glucose. All three mutants showed an identical growth
308 pattern to wild type indicating that the mutants do not contain any additional defects
309 (**Fig. 5A**).

310 Next, the three mutants and wild type were each grown in M9 2% NaCl
311 supplemented with 20 mM *myo*-inositol for 30 h at 28°C (**Fig. 5B**). Under these growth
312 conditions, the Δ*iolT1* mutant had a decreased maximum growth rate of 0.08 h^{-1}
313 compared to wild type; 0.19 h^{-1} and reached a lower final OD_{595} (0.15) as compared to
314 wild type (0.29) (**Fig. 5B**). The Δ*iolT1* mutant also showed a lag time of 6 h compared to
315 3 h for wild type (**Fig. 5B and Fig. S9**). These data indicated that IolT1 is utilized for the
316 transport of *myo*-inositol, but another transporter also transports this compound into
317 the cell. Growth pattern analysis of the Δ*iolX* mutant also showed a decreased growth

318 rate of 0.11 h^{-1} and a lower final OD_{595} of 0.19 compared to wild type, but no difference
319 in the lag phases (**Fig. 5B and Fig. S9**). These data show that IolXYZ is also a *myo*-
320 inositol transporter. Next, we examined the double deletion mutant *iolT1*/*iolX* to
321 determine whether any other transporters could uptake *myo*-inositol. The double
322 mutant failed to grow in M9 supplemented with *myo*-inositol as a sole carbon source
323 showing *V. coralliilyticus* has two *myo*-inositol transporters (**Fig. 5B**). The differences
324 between the lag time of the single mutants, 3 h lag when only *iolT1* was present and a 6
325 h lag for when only *iolX*, indicated that IolT1 is likely more efficient at *myo*-inositol
326 uptake compared to IolXYZ (**Fig. 5B and Fig. S9**).

327 **Phylogenetic analysis of IolG from region 1 and IolA from region 2 among**
328 ***Vibrionaceae* reveals different evolutionary histories.** The low sequence similarity
329 between comparable proteins that are present in both region 1 and 2, and the lack of
330 synteny between the regions suggest different evolutionary histories. To examine this
331 further, a phylogeny based on the IolG protein from region 1 and IolA from region 2
332 were constructed among members of the family *Vibrionaceae* (**Fig. 6 and Fig. S10A**). In
333 addition, a phylogeny based on the housekeeping protein RpoB was also constructed
334 among the same set of species to represent their ancestral relationships and the major
335 clades to which each species belongs (**Fig. S10B)**. To accomplish this, BLAST analysis
336 was first performed using IolG (WP_038162996.1) as a seed to identify homologous
337 protein sequences in the NCBI genome database. A total of 53 sequences with >95%
338 query coverage and >60% amino acid similarity were downloaded and aligned using
339 CLUSTALW (84). The genome context of these IolG proteins within each species was
340 determined to confirm the presence of additional *myo*-inositol metabolism genes.
341 Phylogenetic trees were constructed, and a representative IolG tree is shown in Figure
342 6A constructed using the neighbor-joining method based on evolutionary distance
343 calculated using the JTT matrix-based method (85). IolG was present in 32 *Vibrio*, 11

344 *Photobacterium*, 6 *Enterovibrio* and 4 *Grimontia* species (**Fig. 6A**). Among *Vibrio* species,
345 the IolG proteins were found dispersed within three major clusters on the tree. The *V.*
346 *coralliilyticus* IolG, a species that belongs in the Coralliilyticus clade, branched with high
347 bootstrap value with members of the Mediterranei clade (**Fig. 6A**). Branching distantly
348 from these species was a highly similar cluster of IolG proteins indicated by short
349 branch lengths in species from the Harveyi clade (**Fig. 6A**). Within this tight cluster was
350 IolG from *V. vulnificus*, a species that is not a member of the Harveyi clade (**Fig. 6A** and
351 **Fig. S10B**). These data indicated that IolG and by extension region 1 in *V. vulnificus* was
352 acquired by horizontal gene transfer from a Harveyi clade species. Species in the
353 Harveyi clade did not contain region 2 or a homolog of IolA. The next large clustering
354 of IolG from *Vibrio* species was from four species of the Splendidus clade and branching
355 distantly from these were IolG from nine *Photobacterium* species. Branched distantly
356 from this group were IolG from two *Photobacterium* species that clustered divergently
357 from species from the Cholerae and Splendidus clades (**Fig. 6A and Fig. S10B**). Along
358 with the IolG phylogeny, the differences in gene order and gene content among the
359 *Vibrio* species suggest the *iol* gene clusters have different evolutionary histories and
360 were likely acquired multiple times within the genus (**Fig. 6B**). The IolG proteins from
361 five *Grimontia* species clustered closely together with short branch lengths and identical
362 cluster indicating a single acquisition within the genus (**Fig. 6B**). IolG from species of
363 the genus *Enterovibrio* branched divergently from one another (**Fig. 6A**). Comparisons
364 between the IolG and RpoB trees show that the IolG tree does not follow species
365 evolutionary histories with the exception of *Grimontia* and *Enterovibrio* and indicate that
366 IolG was acquired by horizontal transfer in *Vibrio* and *Photobacterium* species **(Fig.**
367 **S10B**).

368 The IolA protein, a CoA-acylating methylmalonate-semialdehyde
369 dehydrogenase, was selected as the representative of region 2 and used as a seed for

370 BLAST analysis to identify homologs among the *Vibrionaceae*. This analysis uncovered
371 eight *Vibrio* species that contained IolG that did not have a copy of IolA or any of the
372 proteins present in region 2 (**Fig. S10A**). These included species from the Harveyi clade
373 mentioned above as well as *V. astriarenae*, *V. agarivorans*, *V. ponticus*, and *V. vulnificus*. In
374 the IolA tree, the bootstrap values for internal branch nodes for most *Vibrio* and
375 *Photobacterium* species were low and indicated that the relationships of IolA from these
376 species is not clear (**Fig. S10A**). In contrast, the bootstrap values for IolA from *Grimontia*
377 species were robust with short branch lengths and indicated that they are highly related
378 to one another (**Fig. S10A**). Branched divergently from these were IolA from
379 *Enterovibrio* species with greater than 85% confidence in many external nodes and IolA
380 from *V. penaeicida* and *V. nigripulchritudo* also clustered distantly within this group
381 similar to the IolG tree (**Fig. S10A**). The position of IolA from *Photobacterium* species
382 within the tree could not be determined as the internal bootstrap values were < 40%.
383 The IolA protein from *Photobacterium chitinilyticum* branched distantly with IolA from
384 *Vibrio* species similar to IolG from this species. In most *Vibrio* species, divergent
385 branches with long-branch lengths were present, which represented low IolA similarity
386 to each other. Comparisons between the IolG and IolA trees and comparative *iol* cluster
387 analysis suggest that region 1 and 2 were acquired separately, each with a different
388 origin and ancestral history (**Fig. 6 and Fig. S10A**). The phylogeny and *iol* cluster
389 comparisons demonstrate a polyphyletic origin for the *myo*-inositol metabolic clusters
390 likely acquired via horizontal transfer. However, there were no signatures of recent
391 horizontal transfer such as the presence of IS elements, transposases, integrases, phage
392 genes, or plasmid genes within 10 genes of the metabolic gene clusters (with the
393 exception of *V. rumoiensis*, which contained an integrase adjacent to *iolA*).

394 To examine *myo*-inositol metabolism evolutionary history further, an IolG tree
395 was constructed from IolG homologs outside of the *Vibrionaceae* family (**Fig. 7A**). Within

396 this tree, IolG from *Vibrio* species clustered most closely with *Plesiomonas shigelloides* and
397 *Aeromonas* species, both pathogens of fish and humans and clustering divergently from
398 these was IolG from *Providencia* species. A common denominator in all these groups
399 was an 11-13 gene cluster that contained a sodium solute symporter (SSS) type
400 transporter. The *iol* cluster was present in a limited number of strains of *A. allosaccharide*,
401 *A. dhakensis*, *A. finlandensis*, *A. hydrophila*, *A. media*, *A. rivopollensis*, *A. simiae*, and *A.*
402 *taiwanensis.* In *A. dhakensis* strains, also an important pathogen of fish, the *iol* genes were
403 present at a tRNA-Ser locus, within a region that contained phage genes and genes for a
404 restriction modification system (**Fig. 7B**). In *A. media*, *A. allosaccharophila*, and *A.*
405 *finlandersis*, the *iol* gene cluster was also present adjacent to the same tRNA-Ser locus,
406 but had different flanking genes and was present in one strain of each species.

407 In a separate group of *A. hydrophila* strains (>15 strains in the NCBI genome
408 database), the *iol* gene cluster contained the *iolXYZ* transporter. The IolG from these *A.*
409 *hydrophila* strains clustered divergently from other *Aeromonas* species and branched
410 distantly with *Enterobacter* species. These *A. hydrophila* strains were previously
411 characterized as hypervirulent fish pathogens. The *iol* cluster in these strains was
412 inserted adjacent to a tRNA-Leu locus and was surrounded by integrase, transposase,
413 and phage genes, markers of horizontal gene transfer (**Fig. 7B**). Branching divergently
414 from these were IolG from species of the genera *Pectobacterium (formerly Erwinia species),*
415 *Brenneria*, and *Dickeya* (**Fig. 7A**). Genomic analysis of *Brenneria*, *Dickeya*, and
416 *Pectobacterium* showed that the *myo*-inositol metabolic genes were present in a single
417 conserved cluster; in *Pectobacterium* and *Brenneria* the operon structure was
418 *iolADGXYZ_idh_iolCEB* with an ABC-type transporter (*iolXYZ*). In *Dickeya* species, the
419 region was similar to the region in *Pectobacterium* with the exception of three genes
420 inserted between *iolD* and *iolG*. In *Pectobacterium* species, the *iol* cluster was flanked by
421 an addiction system (toxin-antitoxin genes) and the region was located near a tRNA-

422 Asn locus (**Table S2-S5**). In *Brenneria izbisi*, the *iol* region was also located at the same
423 tRNA-Asn locus, but in this species the cluster was flanked by a T6SS and an integrase
424 (**Table S6**). For *Dickeya* and *Pectobacterium*, all species in the IolG tree showed short
425 branch lengths indicating these proteins are highly related to one another within each
426 genus suggesting IolG is ancestral to the genera. This indicates that the region was
427 acquired once, which is also evidenced by their presence at the same genome location
428 (tRNA-Asn).

429 The discovery of inositol catabolism among a relatively small group of *Vibrio*
430 species made us wonder about the distribution of these genes among marine bacteria in
431 general. Previous work by Fuchs and colleagues indicated that *iol* gene clusters were
432 present in over 30 bacterial genera associated with aquatic environments (60). To
433 investigate this further, we examined bacteria associated with different marine hosts for
434 the presence of IolG. This analysis identified *iol* clusters in *Aliiroseovarius*, *Burkholderia*,
435 *Caballeronia*, *Cobetia*, *Endozoicomonas*, *Hahella*, *Halomonas*, *Marinomonas*, *Marinobacterium*,
436 *Labrenzia*, *Marinomonas*, *Marinobacter*, *Oceanspirallaceae*, *Paraburkholderia Pseudomonas*,
437 and *Rhizobia* amongst others (**Fig. 7A**). The IolG phylogeny of these groups showed
438 divergent sequences among closely related species, with species from Alpha-, Beta- and
439 Gamma-Proteobacteria clustered together (**Fig. 7A**). Some genera showed tight
440 clustering of IolG with short branch lengths, such as *Hahella*, *Halomonas*, *Marinomonas*,
441 and *Pseudomonas* (**Fig. S11**). Whereas *Burkholderia* (previously *Pseudomonas*), *Caballeronia*,
442 and *Paraburkholderia* species, all members of the *Burkholderiaceae* family, clustered with
443 each other with short branch lengths and in some cases grouped with *Pseudomonas*
444 species (**Fig. S11**). These genera as well as being significant human and animal
445 pathogens are also characterized as symbionts of protozoa, cnidarians, insects, and
446 plants (86-89). Within the groups that contained an *iol* cluster in our analysis were many
447 genera isolated from reef sponges, corals, marine algae, crustaceans, molluscs and

448 marine fish. For example, *Endozoicomonas*, *Halomonas*, *Inquilinus*, *Labrenzia*, *Roseobacter*,
449 *Pseudomonas*, *Photobacterium*, and *Vibrio* are known symbionts or present in the
450 holobiont of corals (**Fig. S11**) (10, 90, 91). Additionally comparative analysis of the
451 cluster showed common themes such as the presence of a single cluster within which
452 was invariably the ABC-type transporter IolXYZ. A common variation among these
453 clusters was the presence or absence of IolA within the cluster or its presence elsewhere
454 on the genome (**Fig. S12**). Additionally, a difference between these *iol* clusters in marine
455 species compared to the clusters in Enterobacterales (*Brenneria*, *Dickeya*, *Enterobacter*,
456 *Pectobacterium*) was the presence of multiple isomerases and dehydrogenases genes
457 (**Fig. S12**). For example, in *Burkholderia cepacia* four additional dehydrogenase and
458 isomerases were present within the cluster and *Halomonas titanicae*, three additional
459 dehydrogenases and isomerases were present (**Fig. S12**).

460 **DISCUSSION**

461 Our examination of *V. coralliilyticus* response to changes in osmotic stress under
462 different growth temperatures demonstrated the importance of NaCl for optimal
463 growth and growth at high temperatures. The data showed that *V. coralliilyticus* can
464 grow in 1% - 4% NaCl, but grows optimally in 2% NaCl at 28°C and has an absolute
465 requirement for NaCl for growth at 37°C. Compared to other *Vibrio* species such as *V.*
466 *parahaemolyticus* that grow in up to 7% NaCl without the addition of compatible solutes,
467 *V. coralliilyticus* has a relatively low salinity tolerance of 4% NaCl (92-95). A major
468 difference between *V. coralliilyticus* and *V. parahaemolyticus* in their osmotic stress
469 response mechanisms is the absence of the ectoine biosynthesis cluster *ectABC_asp*,
470 which is required for *de novo* biosynthesis of ectoine. Deletion of the ectoine genes in *V.*
471 *parahaemolyticus* inhibited growth in NaCl concentration above 5% NaCl in the absence
472 of exogenous osmolytes (95). *V. coralliilyticus* biosynthesized GB from exogenous
473 choline and transported into the cell a wide range of osmolytes including choline, GB,

474 DMSP, DMG, and ectoine for osmotic protection similar to *V. parahaemolyticus* (92, 93).
475 *Myo*-inositol is a compatible solute more commonly associated with a few
476 hyperthermophile bacteria as well as many eukaryotic species such as algae and plants
477 (96-99). Therefore, it came as no surprise that *V. coralliilyticus* did not use *myo*-inositol
478 for osmotic protection. However, our bioinformatics analysis did identify a genomic
479 region on chromosome 2 in *V. coralliilyticus* that contained *myo*-inositol catabolism gene
480 clusters. This region was present in all *V. coralliilyticus* genomes in the NCBI genome
481 database showing it is a conserved phenotype in this species. Our analysis showed that
482 *V. coralliilyticus* strains can utilize *myo*-inositol as a sole carbon source with a 3 h lag
483 phase. The short lag phase is meaningful because previous studies on *S. enterica* have
484 shown a lag time of over 40 hours (67, 69, 70, 73). *Caulobacter vibrioides* (68, 79),
485 *Rhizobium leguminosarum* (formerly *trifolii*) (74), and *Sinorhizobium meliloti* (100) were
486 also shown to have long lag times of about 14 h when grown on *myo*-inositol as a sole
487 carbon source. A possible reason for this efficient use of *myo*-inositol by *V. coralliilyticus*
488 is the presence of two transporters for uptake into the cell, IolT1 and IolXYZ. As shown
489 in the deletion mutant analysis of these systems, both have somewhat similar *myo*-
490 inositol uptake affinities. Additionally, the regulation of the catabolism genes is likely
491 very different in these divergent species and also control of transport may be different.
492 Our analysis also showed that *V. harveyi* could not utilize *myo*-inositol as a carbon
493 source and this is likely due to the absence of region 2, and IolA specifically. Whether
494 these strains contained region 2 and lost it or never obtained the region is hard to
495 determine but given the high similarity of region 1 among these species the most
496 parsimonious explanation is that region 2 was never acquired. It is possible that the
497 region in *V. harveyi* could be used to metabolize derivatives of inositol.

498 We speculate that during periods of thermal stress, the increased production of
499 inositols by the coral and/or their endosymbiotic algae, as has been shown by Hillyer

500 and colleagues (53), is a metabolic opportunity for bacteria. The ability to consume
501 readily available inositols could provide a selective advantage for *Vibrio* commensal or
502 opportunistic pathogens to increase in abundance within the coral microbiome. In turn,
503 consumption of *myo*-inositol might result in depleting the availability of *myo*-inositol as
504 a stress protectant for algae, which could then lead to a decline in algal survival and
505 abundance. In addition, *myo*-inositol is used as a building block in various signal
506 transduction pathways, and the ability of *V. coralliilyticus* to catabolize this sugar could
507 pose a means for signaling interference. Utilization of predominantly a eukaryotic
508 metabolite could be a side consequence that gives *Vibrio* species a competitive
509 advantage over members of the coral microbiome or other eukaryotic host microbiomes
510 that allows the bacterium to exploit a novel food source and enhance colonization. This
511 competitive advantage could be enhanced during disruption of marine host-microbiota
512 interactions due to thermal, salinity, and/or acidic stresses that change microbial
513 diversity and abundance, similar to the human gut microbiome and human health.

514 Examination of the evolutionary history of IolG showed that the *iol* gene cluster
515 was acquired multiple times within *Vibrionaceae* and given the significant divergence
516 among species, these acquisitions were likely evolutionarily ancient events. Comparison
517 of the IolG and IolA trees showed they were not congruent indicating the two regions
518 were acquired separately. The closest relative to IolG outside of the Vibrionales were a
519 few members of the Aeromonadales (*Aeromonas*) and many Enterobacterales from the
520 genera *Brenneria*, *Dickeya*, *Enterobacteria*, *Pectobacterium*, *Plesiomonas*, *Providencia*. The
521 history of the region among these groups was very different, with signatures of
522 horizontal transfer present among *Aeromonas* species. *Aeromonas* are found in fresh and
523 marine water environments and include many species pathogenic to fish and humans.
524 Two different *myo*-inositol clusters were present in *Aeromonas* species, each containing a
525 single cluster. IolG from seven *Aeromonas* species and from *Plesiomonas shigelloides*

526 branched with IolG from *Vibrio* species and the *iol* cluster in these species encoded a
527 sodium solute symporter (SSS). *P. shigelloides* is the sole member of the genus and is
528 predominantly isolated from aquatic environments and their inhabitants. *P. shigelloides*
529 is presently within the family *Enterobacteriaceae,* but was previously a member of the
530 family *Vibrionaceae* and then *Aeromonadaceae* and has been described as a fish and
531 human pathogen (101). The *iol* cluster is present in all *P. shigelloides* genomes in the
532 NCBI database (as of March 2024) and this species has been shown to utilize *myo*-
533 inositol as a carbon source (101). Included in this IolG group were two *A. hydrophila*
534 strains WCX23 and 23-C-23, where the *iol* metabolic cluster was flanked on both ends
535 by genes encoding a type six secretion system (T6SS) and was inserted next to a tRNA-
536 His locus (**Fig. 7B**). In *A. dhakensis* and the other five species, the *iol* cluster was located
537 adjacent to a tRNA-Ser locus and flanked by signatures of mobile elements (**Fig. 7B**). In
538 hypervirulent *A. hydrophila* strains associated with epidemic disease in fish aquaculture
539 farms in China and the USA, the single *iol* cluster contained the IolXYZ ABC-type
540 transporter and clustered with IolG from *Enterobacter* species. In these hypervirulent *A.*
541 *hydrophila*, the *iol* cluster was flanked by an integrase and phage genes on one end and
542 an IS3 element on the opposite end and was inserted at a tRNA-Leu locus. Previous
543 studies showed that hypervirulent *A. hydrophila* strains all contained an *iol* cluster, could
544 utilize *myo*-inositol as a sole carbon source, and was an important trait differentiating
545 these strains from other *A. hydrophila* isolates (102-104). *Enterobacter* species are
546 ubiquitous in nature, present in soil and water, and are well known plant pathogens
547 and opportunistic pathogens of humans (105). Several species of *Enterobacter* have been
548 shown to utilize *myo*-inositol as a carbon source (105). Nested within IolG from
549 *Enterobacter* species was IolG from a single *A. taiwanensis* strain. However, the genome
550 for this species was incomplete so the genome context could not be explored further.
551 Overall, the data suggest that in *Aeromonas*, the *iol* gene cluster is a recent addition
552 acquired multiple times on mobile genetic elements and may have contributed to the

553 emergence of hypervirulent *Aeromonas* fish pathogens. Distantly related to these was
554 IolG from *Pectobacterium*, *Brenneria*, and *Dickeya* species which are broad host range
555 pathogens of plants with a worldwide distribution (**Fig. 7**) (106, 107). The *iol* cluster was
556 universally present in these genera suggesting it is a key phenotype of the group.
557 Emerging evidence from plant rhizosphere studies recently demonstrated that plant-
558 produced inositol catabolized by bacteria correlated with their higher root colonization
559 (108, 109). Whether the presence of *myo*-inositol catabolism genes aids in pathogen's
560 colonization of plants or is a beneficial trait picked up to take advantage of plant disease
561 releasing inositols remains to be determined. Our analysis also showed that the *iol*
562 cluster is present among a diverse range of marine species (**Fig. S11**). This is in
563 agreement with Fuchs and colleagues demonstrating that over 30 bacterial genera from
564 aquatic environments contained *iol* clusters (60). Many of these species are associated
565 with marine hosts including endosymbionts of corals (110, 111). The distribution of the
566 *iol* cluster within many genera was not universal, suggesting a possible role in niche
567 partitioning.

568 **MATERIALS AND METHODS**

569 **Bacterial strains, media, and culture conditions**. All strains and plasmids used in this
570 study are listed in **Table 1**. Four *Vibrio coralliilyticus* strains were examined in this study,
571 strains CN52H-1, OCN014, BAA-450, and RE87. Unless stated otherwise, *V.*
572 *coralliilyticus* was grown at 28°C in either lysogeny broth (LB) (Fisher Scientific, Fair
573 Lawn, NJ) with 2% (wt/vol) NaCl (LB 2%NaCl) or M9 minimal media (47.8 mM
574 Na_2HPO_4, 22 mM KH_2PO_4, 18.7 mM NH_4Cl, 8.6 mM NaCl; Sigma Aldrich)
575 supplemented with 2 mM $MgSO_4$, 0.1 mM $CaCl_2$, 2% (wt/vol) NaCl and 20 mM glucose
576 as the sole carbon source (M9G 2% NaCl). *Escherichia coli* strains were grown in LB
577 supplemented with 1% (wt/vol) NaCl (LB1%) at 37°C. The strain *E. coli* β2155 *λpir* is a
578 diaminopimelic acid (DAP) auxotroph and was grown supplemented with 0.3 mM

579 DAP (112). The *V. harveyi* strain used for analysis was strain 393 (113). Chloramphenicol
580 (Cm) was added to media at a concentration of 12.5 μg/mL when specified.

581 **Osmotic Stress Growth Analysis**. *Vibrio coralliilyticus* was grown overnight in M9G 1%
582 NaCl at 28°C with aeration. A 2% inoculation of the overnight culture into fresh M9G
583 1% NaCl was grown to OD_{595} of ~ 0.50 at 28°C with aeration. Exponential cultures were
584 inoculated 1:40 into 200 μL fresh M9G media containing 1% to 6% NaCl. When using
585 compatible solutes glycine betaine (GB), dimethylsulfoniopropionate (DMSP), ectoine,
586 choline, dimethylglycine (DMG), trimethylamine N-oxide (TMAO), gamma-
587 aminobutyric acid (GABA), creatine, *myo*-inositol (MI), and glycerol were used at a final
588 concentration of 1 mM in M9G 5% NaCl. Plates were incubated at 28°C with
589 intermittent shaking for 1 min every hour. Optical densities were taken at 595 nm every
590 hour for a total of 24 h using a Tecan Sunrise microplate reader and Magellan plate
591 reader software (Tecan Systems Inc., San Jose, CA).

592 **Deletion Mutant Construction**. In-frame non-polar deletion mutants of *iolG*
593 (HRJ43_RS06535), *iolT1* (HRJ43_RS06585), and *iolX* (HRJ43_RS06670) were constructed
594 using SOE PCR and allelic exchange as previously described (114). Truncations of the
595 genes of interest, *iolG* (18-bp of the 984-bp gene), *iolT1* (30-bp of the 1452-bp gene), and
596 *iolX* (24-bp of the 1008-bp gene) were generated using the primers listed in **Table 2**. The
597 truncated gene products were ligated with the suicide vector pDS132 using the Gibson
598 assembly protocol and then transformed into *E. coli* Dh5α λpir (115, 116). The plasmids
599 pDSΔ*iolG*, pDSΔ*iolT1*, and pDSΔ*iolX* were then purified and transformed into *E. coli*
600 β2155 *λpir* (DAP auxotroph). Then conjugation followed by homologous recombination
601 into the *V. coralliilyticus* CN52H-1 genome was completed. To select for the single
602 crossover of the plasmids into the genome, plating onto chloramphenicol (Cm) was
603 used and colonies were screened via PCR for the truncated allele. To induce a double-
604 crossover event, the single-cross strains were grown overnight in the absence of Cm.

605 The cultures were then spread on 10% sucrose plates, and healthy colonies were
606 screened for gene truncation, and plasmid excision. Colonies that still contained the
607 plasmid would appear soupy on the 10% sucrose plates because of the presence of *sacB*
608 selectable marker. In-frame deletions were confirmed with sequencing.

609 **Metabolic Growth Analysis**. Strains were grown overnight in M9G 2% NaCl at 28°C
610 with aeration. Overnight cultures were washed twice with PBS and then inoculated 1:40
611 into 200 μL fresh M9 media supplemented with 2% NaCl, and a specified carbon source
612 (glucose (20 mM) or *myo*-inositol (20 mM)). Plates were incubated at 28°C with
613 intermittent shaking for 1 min every hour. Optical densities were taken at 595 nm
614 hourly for a total of 30 h using a Tecan Sunrise microplate reader and Magellan plate
615 reader software (Tecan Systems Inc., San Jose, CA).

616 **Preparation of cellular extracts and proton nuclear magnetic resonance (^{1}H-NMR)**.
617 Wild type *V. coralliilyticus* was grown overnight at 28°C in M9G 4% NaCl supplemented
618 with 1 mM choline. Stationary phase cells were pelleted and washed twice with PBS.
619 Three freeze-thaw cycles were performed with the cell pellets to increase lysis, and the
620 cells were resuspended in 750 μL ethanol. Debris was pelleted by centrifugation, and
621 the ethanol solution was transferred to a clean tube and evaporated under vacuum. The
622 pellet was resuspended in deuterium oxide (D_2O), and insoluble material was removed
623 by centrifugation. The solution was transferred to a 5-mm NMR tube for analysis on a
624 Bruker AVANCE 600NMR spectrometer at a proton frequency of 600.13 MHz with a
625 sweep of 12,376 Hz and a relaxation delay of 5 s. Sixteen scans were co-added for each
626 spectrum.

627 **Phylogenetic analysis**. Phylogenetic analysis was conducted using the program MEGA
628 X (117). The evolutionary history of IolG, IolA and RpoB was inferred using the
629 Neighbor-Joining method (118). The evolutionary distances were computed using the
630 Jones-Taylor-Thornton (JTT) matrix-based method and are in the units of the number of

631 amino acid substitutions per site (85). All ambiguous positions were removed for each
632 sequence pair (pairwise deletion option).

633 **Ligand Docking Modeling**. The transporter amino acid sequences were downloaded
634 from NCBI and aligned using ClustalW(84): *B. subtilis* IolT (WP_003234027.1), *S. enterica*
635 IolT1 (NP_463279.1), *V. coralliilyticus* IolT1 (WP_099607352.1), *V. coralliilyticus* IolT2
636 (WP_172853823.1), *C. crescentus* IbpA (WP_010918744.1), and *V. coralliilyticus* IolX
637 (WP_227495657.1). Transporter alignments were displayed and annotated using ESPript
638 (http://espript.ibcp.fr/ESPript/cgi-bin/ESPript.cgi) (119). Predicted protein structures
639 were obtained from AlphaFold (120). The Ligand model for *myo*-inositol (MI) was
640 obtained from Chemical Entities of Biological Interest (CheBI) EMBL (121). Polar
641 hydrogens were added to the ligand structures. The docking experiments were
642 performed using SeamDock which was set to use docking parameters for the Vina
643 software (Spacing: 1.0, Mode: 2, Energy Range: 5, Exhaustiveness: 8) (122).

644 **Data Availability.** All datasets are available upon request.

645 **ACKNOWLEDGEMENTS**

646 This research was supported in part by a National Science Foundation grant (award
647 IOS-1656688) to E.F.B. KBL was funded in part by the Chemistry-Biology Interface
648 predoctoral training program grant: 5T32GM008550.

649 **Figure Legends**

650 **Fig. 1. Pathway of m*yo*-inositol catabolism.** The pathway presented is based upon
651 enzymological studies in *B. subtilis* and genome comparison. Enzymes (red) and
652 intermediate compounds in the pathway are displayed.

653 **Fig. 2. *Vibrio coralliilyticus* NaCl and temperature tolerance range.** Growth curves of
654 *V. coralliilyticus* strains in minimal media (M9) with glucose (M9G) and a final
655 concentration of 1% to 6% NaCl. Growth was measured every hour for 24 h at **A.** 28°C
656 strain CN52H-1, **B.** 37°C strain CN52H-1, **C.** 28°C strain OCN014, **D.** 37°C strain
657 OCN014, **E.** 28°C strain BAA-450, **F.** 37°C strain BAA-450, **G.** 28°C strain RE-87, **H.** 37°C
658 strain RE-87. Mean and standard deviation of three biological replicates are shown.

659 **Fig. 3. *V. coralliilyticus* compatible solute biosynthesis and uptake systems. A.** ^{1}H-
660 NMR spectra of *V. coralliilyticus* CN52H-1 cellular extract grown in minimal media
661 (M9G) 4% NaCl without choline and **B**. with the addition of 1 mM choline. The spectral
662 peaks corresponding to glycine betaine are labeled with red asterisks. **C.** *V. coralliilyticus*
663 was inoculated into M9G 5% NaCl with 1 mM GB (glycine betaine), DMSP
664 (dimethylsulfoniopropionate), ectoine, choline, MI (*myo*-inositol), DMG
665 (dimethylglycine), trimethylamine N-oxide (TMAO), gamma-aminobutyric acid
666 (GABA), creatine, or glycerol. Growth was measured for 24 h at 28°C and the calculated
667 area under the curve calculated. Final OD is shown above each compatible solute that
668 rescued growth. Mean and standard deviation of three biological replicates are shown.

669 **Fig. 4. *V. coralliilyticus* utilized *myo*-inositol as a sole carbon source. A.** Schematic of
670 the gene order of *myo*-inositol transporter, catabolism and regulatory genes in *V.*
671 *coralliilyticus*. **B.** Growth curve analysis in minimal media (M9 2% NaCl) containing
672 either 20 mM glucose (squares) or 20 mM *myo*-inositol (MI, triangles) or no carbon
673 source (circles) for *V. coralliilyticus* CN52H-1. **C.** *V. coralliilyticus* strains OCN014, BAA-
674 450, and RE87. **D.** *V. harveyi* 393 and **E**. *V. coralliilyticus* Δ*iolG.* Growth was measured
675 every hour for 30 h at 28°C. Mean and standard deviation of four biological replicates
676 are shown.

677 **Fig. 5. Growth pattern analysis of *V. coralliilyticus myo*-inositol transporters deletion**
678 **mutants.** Growth curves of wild type, Δ*iolT1*, Δ*iolX*, and Δ*iolT1*/ Δ*iolX* in minimal media

679 (M9 2% NaCl) with **A.** 20 mM glucose or **B.** 20 mM *myo*-inositol as a sole carbon source.
680 Growth was measured every hour for 30 h at 28°C. Mean and standard deviation of
681 three biological replicates are shown.

682 **Fig. 6. Phylogenetic distribution of IolG and Iol cluster organization among**
683 ***Vibrionaceae*. A.** IolG evolutionary history was inferred using the Neighbor-Joining
684 method (118) with bootstrap value of 1000 (123). The optimal tree with the sum of
685 branch length = 4.11930205 is shown. The tree is drawn to scale, and evolutionary
686 distances were computed using the JTT matrix-based method (85) with units of the
687 number of amino acid substitutions per site. Shown are 53 amino acid sequences,
688 ambiguous positions were removed for each sequence pair (pairwise deletion option)
689 with a total of 332 positions. Evolutionary analyses were conducted in MEGA X (117).
690 IolG was present in 32 *Vibrio* (red), 11 *Photobacterium* (blue), 6 *Enterovibrio* (orange), and
691 4 *Grimontia* (brown) species. **B**. Iol cluster organization among *Vibrionaceae* species.
692 Arrows represent open reading frame and direction of transcription, slanted double
693 black lines represent genes between regions.

694 **Fig. 7. IolG phylogeny among marine species.** Condensed consensus tree with
695 collapsed branches is shown, original tree is shown in **Fig. S11**. IolG phylogeny was
696 inferred using the Neighbor-Joining method (118). The bootstrap test (1000 replicates)
697 are shown next to the branches. This analysis involved 358 amino acid sequences. Blue
698 and red collapsed branches represent Gamma-, purple represents Beta-, and green
699 represents Alpha-Proteobacteria. **B.** Genome context of *myo*-inositol metabolism clusters
700 within mobile genetic elements in *Aeromonas* species.

701

702 **Table 1. Strains and plasmids used in this study**

Strain/plasmid	Genotype or description	Reference/source
Vibrio coralliilyticus		
CN52H-1	Environmental isolate from reef coral	(16)
OCN014	Pathogen of the coral *Acropora cytherea*	(23)
BAA-450	Pathogen of the coral *Pocillopora damicornis*	(19)
RE87 (00-90-6)	Isolated from diseased Pacific oyster larvae	(80, 81)
Δ*iolG*	Deletion of HRJ43_RS06535 from CN52H-1	This study
Δ*iolT1*	Deletion of HRJ43_RS06585 from CN52H-1	This study
Δ*iolX*	Deletion of HRJ43_RS06670 from CN52H-1	This study
Δ*iolT1*/Δ*iolX*	*iolX* deletion in Δ*iolT2* mutant background	This study
Vibrio harveyi		
393	Isolated from barramundi in Australia	(113)
Escherichia coli		
DH5α *λpir*		ThermoFisher Scientific
B2155 *λpir*	Δ*dapA*::erm pir for bacterial conjugation	(112)
Plasmids		
pDS132	Suicide plasmid; CmR; *sacB*, R6Kg ori	(116)
pDS*iolG*	pDS132 harboring truncated *iolG* allele	This study
pDS*iolT1*	pDS132 harboring truncated *iolT1* allele	This study
pDS*iolX*	pDS132 harboring truncated *iolX* allele	This study

703

704

705

706 **Table 2. Primers used in this study**

Primer Name	Sequence (5′ – 3′)	Length (bp)
Mutant Primers		
AB fwd_*iolG*	accgcatgcgatatcgagctGTGGTTGAGGTGTACACC	549
AB rev_*iolG*	cttatagtgaATTAAACATTCTGTACTCCTTACAG	
CD fwd_*iolG*	aatgtttaatTCACTATAAGAAATTCAACCGGAAG	549
CD rev_*iolG*	gtggaattcccgggagagctTCCGGAAATCGTCCGCTATTTC	
flank fwd_*iolG*	acatcggtcagcgtatgtct	2369
flank rev_*iolG*	aaccgcgactacctttacca	
AB fwd_*iolT1*	accgcatgcgatatcgagctATGCTTTTCATCTCTCGTTC	549
AB rev_*iolT1*	gtacgtgcgcATGACTCGATGACATGTTTC	
CD fwd_*iolT1*	atcgagtcatGCGCACGTACAATAACATTG	549
CD rev_*iolT1*	gtggaattcccgggagagctCGATACCCCTGAAATGAGG	
flank fwd_*iolT1*	actttgttcccagctccgta	2809
flank rev_*iolT1*	gcgaacaaacaatggtgctg	
AB fwd_*iolX*	accgcatgcgatatcgagctCAACTATCGCCGAATAAGGTTATTTG	606
AB rev_*iolX*	aacctttttgTAATGATGGCATCATTGCC	
CD fwd_*iolX*	gccatcattaCAAAAAGGTTAATGGAATAACAGC	465
CD rev_*iolX*	gtggaattcccgggagagctATCGCGATACATCTTATCGTG	
flank fwd_*iolX*	cgatgacccaccgagatact	2248
flank rev_*iolX*	caccgtcagttcagtcatcg	

707

708

REFERENCES

1. Kushmaro A, Rosenberg E, Fine M, Loya Y. 1997. Bleaching of the coral Oculina patagonica by Vibrio AK-1. Marine Ecology Progress Series 147:159-165.
2. Ben-Haim Y, Zicherman-Keren M, Rosenberg E. 2003. Temperature-regulated bleaching and lysis of the coral Pocillopora damicornis by the novel pathogen Vibrio coralliilyticus. Appl Environ Microbiol 69:4236-42.
3. Munn CB. 2015. The Role of Vibrios in Diseases of Corals. Microbiol Spectr 3(4).
4. Arotsker L, Siboni N, Ben-Dov E, Kramarsky-Winter E, Loya Y, Kushmaro A. 2009. Vibrio sp. as a potentially important member of the Black Band Disease (BBD) consortium in Favia sp. corals. FEMS Microbiol Ecol 70:515-24.
5. Vezzulli L, Previati M, Pruzzo C, Marchese A, Bourne DG, Cerrano C. 2010. Vibrio infections triggering mass mortality events in a warming Mediterranean Sea. Environ Microbiol 12:2007-19.
6. Vidal-Dupiol J, Ladrière O, Meistertzheim AL, Fouré L, Adjeroud M, Mitta G. 2011. Physiological responses of the scleractinian coral Pocillopora damicornis to bacterial stress from Vibrio coralliilyticus. J Exp Biol 214:1533-45.
7. Rubio-Portillo E, Yarza P, Peñalver C, Ramos-Esplá AA, Antón J. 2014. New insights into Oculina patagonica coral diseases and their associated Vibrio spp. communities. Isme j 8:1794-807.
8. Rubio-Portillo E, Martin-Cuadrado AB, Caraballo-Rodríguez AM, Rohwer F, Dorrestein PC, Antón J. 2020. Virulence as a Side Effect of Interspecies Interaction in Vibrio Coral Pathogens. mBio 11(4):e00201-20.
9. Moriarty T, Leggat W, Huggett MJ, Ainsworth TD. 2020. Coral Disease Causes, Consequences, and Risk within Coral Restoration. Trends Microbiol 28:793-807.
10. Voolstra CR, Raina JB, Dörr M, Cárdenas A, Pogoreutz C, Silveira CB, Mohamed AR, Bourne DG, Luo H, Amin SA, Peixoto RS. 2024. The coral microbiome in sickness, in health and in a changing world. Nat Rev Microbiol https://doi.org/10.1038/s41579-024-01015-3.
11. Santos Ede O, Alves N, Jr., Dias GM, Mazotto AM, Vermelho A, Vora GJ, Wilson B, Beltran VH, Bourne DG, Le Roux F, Thompson FL. 2011. Genomic and proteomic analyses of the coral pathogen Vibrio coralliilyticus reveal a diverse virulence repertoire. Isme j 5:1471-83.
12. Kooperman N, Ben-Dov E, Kramarsky-Winter E, Barak Z, Kushmaro A. 2007. Coral mucus-associated bacterial communities from natural and aquarium environments. FEMS Microbiol Lett 276:106-13.
13. Kimes NE, Grim CJ, Johnson WR, Hasan NA, Tall BD, Kothary MH, Kiss H, Munk AC, Tapia R, Green L, Detter C, Bruce DC, Brettin TS, Colwell RR, Morris PJ. 2012. Temperature regulation of virulence factors in the pathogen Vibrio coralliilyticus. Isme j 6:835-46.
14. Godwin S, Bent E, Borneman J, Pereg L. 2012. The role of coral-associated bacterial communities in Australian Subtropical White Syndrome of Turbinaria mesenterina. PLoS One 7:e44243.
15. Ushijima B, Saw JH, Videau P, Häse CC. 2022. Comparison of Vibrio coralliilyticus virulence in Pacific oyster larvae and corals. Microbiology (Reading) 168(4).
16. Ushijima B, Meyer JL, Thompson S, Pitts K, Marusich MF, Tittl J, Weatherup E, Reu J, Wetzell R, Aeby GS, Häse CC, Paul VJ. 2020. Disease Diagnostics and Potential Coinfections by Vibrio coralliilyticus During an Ongoing Coral Disease Outbreak in Florida. Front Microbiol 11:569354.
17. Ben-Haim Y, Rosenberg E. 2002. A novel Vibrio sp. pathogen of the coral Pocillopora damicornis. Marine Biology 141:47-55.

754 18. Rosenberg E, Ben-Haim Y. 2002. Microbial diseases of corals and global warming. Environ
755 Microbiol 4:318-26.
756 19. Ben-Haim Y, Thompson FL, Thompson CC, Cnockaert MC, Hoste B, Swings J, Rosenberg E. 2003.
757 Vibrio coralliilyticus sp. nov., a temperature-dependent pathogen of the coral Pocillopora
758 damicornis. Int J Syst Evol Microbiol 53:309-315.
759 20. Bourne DG, Munn CB. 2005. Diversity of bacteria associated with the coral Pocillopora
760 damicornis from the Great Barrier Reef. Environ Microbiol 7:1162-74.
761 21. Sussman M, Willis BL, Victor S, Bourne DG. 2008. Coral pathogens identified for White Syndrome
762 (WS) epizootics in the Indo-Pacific. PLoS One 3:e2393.
763 22. Ushijima B, Videau P, Burger AH, Shore-Maggio A, Runyon CM, Sudek M, Aeby GS, Callahan SM.
764 2014. Vibrio coralliilyticus strain OCN008 is an etiological agent of acute Montipora white
765 syndrome. Appl Environ Microbiol 80:2102-9.
766 23. Ushijima B, Videau P, Poscablo D, Stengel JW, Beurmann S, Burger AH, Aeby GS, Callahan SM.
767 2016. Mutation of the toxR or mshA genes from Vibrio coralliilyticus strain OCN014 reduces
768 infection of the coral Acropora cytherea. Environ Microbiol 18:4055-4067.
769 24. Richards GP, Watson MA, Needleman DS, Church KM, Häse CC. 2015. Mortalities of Eastern and
770 Pacific oyster Larvae caused by the pathogens Vibrio coralliilyticus and Vibrio tubiashii. Appl
771 Environ Microbiol 81:292-7.
772 25. Ushijima B, Richards GP, Watson MA, Schubiger CB, Häse CC. 2018. Factors affecting infection of
773 corals and larval oysters by Vibrio coralliilyticus. PLoS One 13:e0199475.
774 26. Richards GP, Watson MA, Madison D, Soffer N, Needleman DS, Soroka DS, Uknalis J, Baranzoni
775 GM, Church KM, Polson SW, Elston R, Langdon C, Sulakvelidze A. 2021. Bacteriophages against
776 Vibrio coralliilyticus and Vibrio tubiashii: Isolation, Characterization, and Remediation of Larval
777 Oyster Mortalities. Appl Environ Microbiol 87(10):e00008-21.
778 27. Kim HJ, Giri SS, Kim SG, Kim SW, Kwon J, Lee SB, Park SC. 2020. Isolation and Characterization of
779 Two Bacteriophages and Their Preventive Effects against Pathogenic Vibrio coralliilyticus
780 Causing Mortality of Pacific Oyster (Crassostrea gigas) Larvae. Microorganisms 8(6):926.
781 28. Kim HJ, Jun JW, Giri SS, Chi C, Yun S, Kim SG, Kim SW, Han SJ, Kwon J, Oh WT, Lee SB, Kim JH,
782 Park SC. 2020. Identification and Genome Analysis of Vibrio coralliilyticus Causing Mortality of
783 Pacific Oyster (Crassostrea gigas) Larvae. Pathogens 9(3):206.
784 29. Richards GP, Kingham BF, Shevchenko O, Watson MA, Needleman DS. 2018. Complete Genome
785 Sequence of Vibrio coralliilyticus RE22, a Marine Bacterium Pathogenic toward Larval Shellfish.
786 Microbiol Resour Announc 7(17):e01332-18.
787 30. Vega Thurber R, Willner-Hall D, Rodriguez-Mueller B, Desnues C, Edwards RA, Angly F, Dinsdale
788 E, Kelly L, Rohwer F. 2009. Metagenomic analysis of stressed coral holobionts. Environ Microbiol
789 11:2148-63.
790 31. Tout J, Siboni N, Messer LF, Garren M, Stocker R, Webster NS, Ralph PJ, Seymour JR. 2015.
791 Increased seawater temperature increases the abundance and alters the structure of natural
792 Vibrio populations associated with the coral Pocillopora damicornis. Front Microbiol 6:432.
793 32. Garren M, Son K, Tout J, Seymour JR, Stocker R. 2016. Temperature-induced behavioral switches
794 in a bacterial coral pathogen. Isme j 10:1363-72.
795 33. Gibbin E, Gavish A, Krueger T, Kramarsky-Winter E, Shapiro O, Guiet R, Jensen L, Vardi A,
796 Meibom A. 2019. Vibrio coralliilyticus infection triggers a behavioural response and perturbs
797 nutritional exchange and tissue integrity in a symbiotic coral. Isme j 13:989-1003.
798 34. Welsh RM, Rosales SM, Zaneveld JR, Payet JP, McMinds R, Hubbs SL, Vega Thurber RL. 2017.
799 Alien vs. predator: bacterial challenge alters coral microbiomes unless controlled by
800 Halobacteriovorax predators. PeerJ 5:e3315.

801 35. Rosado PM, Leite DCA, Duarte GAS, Chaloub RM, Jospin G, Nunes da Rocha U, J PS, Dini-
802 Andreote F, Eisen JA, Bourne DG, Peixoto RS. 2019. Marine probiotics: increasing coral
803 resistance to bleaching through microbiome manipulation. Isme j 13:921-936.
804 36. Kopp C, Domart-Coulon I, Escrig S, Humbel BM, Hignette M, Meibom A. 2015. Subcellular
805 investigation of photosynthesis-driven carbon assimilation in the symbiotic reef coral
806 Pocillopora damicornis. mBio 6(1):e02299-14.
807 37. Sproles AE, Kirk NL, Kitchen SA, Oakley CA, Grossman AR, Weis VM, Davy SK. 2018. Phylogenetic
808 characterization of transporter proteins in the cnidarian-dinoflagellate symbiosis. Mol
809 Phylogenet Evol 120:307-320.
810 38. Matthews JL, Oakley CA, Lutz A, Hillyer KE, Roessner U, Grossman AR, Weis VM, Davy SK. 2018.
811 Partner switching and metabolic flux in a model cnidarian-dinoflagellate symbiosis. Proc Biol Sci
812 285(1892):20182336.
813 39. LaJeunesse TC, Thornhill DJ, Cox EF, Stanton FG, Fitt WK, Schmidt GW. 2004. High diversity and
814 host specificity observed among symbiotic dinoflagellates in reef coral communities from
815 Hawaii. Coral Reefs 23:596-603.
816 40. Tanaka Y, Miyajima T, Koike I, Hayashibara T, Ogawa H. 2006. Translocation and conservation of
817 organic nitrogen within the coral-zooxanthella symbiotic system of Acropora pulchra, as
818 demonstrated by dual isotope-labeling techniques. Journal of Experimental Marine Biology and
819 Ecology 336:110-119.
820 41. Rädecker N, Pogoreutz C, Voolstra CR, Wiedenmann J, Wild C. 2015. Nitrogen cycling in corals:
821 the key to understanding holobiont functioning? Trends Microbiol 23:490-7.
822 42. Rosic N, Ling EY, Chan CK, Lee HC, Kaniewska P, Edwards D, Dove S, Hoegh-Guldberg O. 2015.
823 Unfolding the secrets of coral-algal symbiosis. Isme j 9:844-56.
824 43. Cui G, Liew YJ, Konciute MK, Zhan Y, Hung SH, Thistle J, Gastoldi L, Schmidt-Roach S, Dekker J,
825 Aranda M. 2022. Nutritional control regulates symbiont proliferation and life history in coral-
826 dinoflagellate symbiosis. BMC Biol 20:103.
827 44. Rands ML, Loughman BC, Douglas AE. 1993. The Symbiotic Interface in an Alga-Invertebrate
828 Symbiosis. Proceedings: Biological Sciences 253:161-165.
829 45. Muscatine L, Porter JW. 1977. Reef Corals: Mutualistic Symbioses Adapted to Nutrient-Poor
830 Environments. BioScience 27:454-460.
831 46. Aranda M, Li Y, Liew YJ, Baumgarten S, Simakov O, Wilson MC, Piel J, Ashoor H, Bougouffa S,
832 Bajic VB, Ryu T, Ravasi T, Bayer T, Micklem G, Kim H, Bhak J, LaJeunesse TC, Voolstra CR. 2016.
833 Genomes of coral dinoflagellate symbionts highlight evolutionary adaptations conducive to a
834 symbiotic lifestyle. Sci Rep 6:39734.
835 47. LaJeunesse TC, Parkinson JE, Gabrielson PW, Jeong HJ, Reimer JD, Voolstra CR, Santos SR. 2018.
836 Systematic Revision of Symbiodiniaceae Highlights the Antiquity and Diversity of Coral
837 Endosymbionts. Curr Biol 28:2570-2580.e6.
838 48. Ashley IA, Kitchen SA, Gorman LM, Grossman AR, Oakley CA, Suggett DJ, Weis VM, Rosset SL,
839 Davy SK. 2022. Genomic conservation and putative downstream functionality of the
840 phosphatidylinositol signalling pathway in the cnidarian-dinoflagellate symbiosis. Front
841 Microbiol 13:1094255.
842 49. Michell RH. 2008. Inositol derivatives: evolution and functions. Nat Rev Mol Cell Biol 9:151-61.
843 50. Majumder AL, Chatterjee A, Ghosh Dastidar K, Majee M. 2003. Diversification and evolution of
844 L-myo-inositol 1-phosphate synthase. FEBS Lett 553:3-10.
845 51. Turner BL, Papházy MJ, Haygarth PM, McKelvie ID. 2002. Inositol phosphates in the
846 environment. Philos Trans R Soc Lond B Biol Sci 357:449-69.

847 52. Lehnert EM, Mouchka ME, Burriesci MS, Gallo ND, Schwarz JA, Pringle JR. 2014. Extensive
848 differences in gene expression between symbiotic and aposymbiotic cnidarians. G3 (Bethesda)
849 4:277-95.
850 53. Hillyer KE, Dias DA, Lutz A, Roessner U, Davy SK. 2017. Mapping carbon fate during bleaching in
851 a model cnidarian symbiosis: the application of (13) C metabolomics. New Phytol 214:1551-
852 1562.
853 54. Blatt MR, Thiel G, Trentham DR. 1990. Reversible inactivation of K+ channels of Vicia stomatal
854 guard cells following the photolysis of caged inositol 1,4,5-trisphosphate. Nature 346:766-9.
855 55. Thiel G, MacRobbie EA, Hanke DE. 1990. Raising the intracellular level of inositol 1,4,5-
856 trisphosphate changes plasma membrane ion transport in characean algae. Embo j 9:1737-41.
857 56. Al-Mushhin AAM, Qari SH, Fakhr MA, Alnusairi GSH, Alnusaire TS, AA AL, Latef A, Ali OM, Khan
858 AA, Soliman MH. 2021. Exogenous Myo-Inositol Alleviates Salt Stress by Enhancing Antioxidants
859 and Membrane Stability via the Upregulation of Stress Responsive Genes in Chenopodium
860 quinoa L. Plants (Basel) 10(11):2416.
861 57. Das-Chatterjee A, Goswami L, Maitra S, Dastidar KG, Ray S, Majumder AL. 2006. Introgression of
862 a novel salt-tolerant L-myo-inositol 1-phosphate synthase from Porteresia coarctata (Roxb.)
863 Tateoka (PcINO1) confers salt tolerance to evolutionary diverse organisms. FEBS Lett 580:3980-
864 8.
865 58. Nelson DE, Koukoumanos M, Bohnert HJ. 1999. Myo-inositol-dependent sodium uptake in ice
866 plant. Plant Physiol 119:165-72.
867 59. Gillaspy GE. 2011. The cellular language of myo-inositol signaling. New Phytol 192:823-839.
868 60. Weber M, Fuchs TM. 2022. Metabolism in the Niche: a Large-Scale Genome-Based Survey
869 Reveals Inositol Utilization To Be Widespread among Soil, Commensal, and Pathogenic Bacteria.
870 Microbiol Spectr 10:e0201322.
871 61. Felsl A, Brokatzky D, Kröger C, Heermann R, Fuchs TM. 2023. Hierarchic regulation of a
872 metabolic pathway: H-NS, CRP, and SsrB control myo-inositol utilization by Salmonella enterica.
873 Microbiol Spectr:e0272423.
874 62. Yoshida KI, Aoyama D, Ishio I, Shibayama T, Fujita Y. 1997. Organization and transcription of the
875 myo-inositol operon, iol, of Bacillus subtilis. J Bacteriol 179:4591-8.
876 63. Yoshida K, Yamamoto Y, Omae K, Yamamoto M, Fujita Y. 2002. Identification of two myo-inositol
877 transporter genes of Bacillus subtilis. J Bacteriol 184:983-91.
878 64. Yoshida K, Yamaguchi M, Morinaga T, Kinehara M, Ikeuchi M, Ashida H, Fujita Y. 2008. myo-
879 Inositol catabolism in Bacillus subtilis. J Biol Chem 283:10415-24.
880 65. Yoshida KI, Sanbongi A, Murakami A, Suzuki H, Takenaka S, Takami H. 2012. Three inositol
881 dehydrogenases involved in utilization and interconversion of inositol stereoisomers in a
882 thermophile, Geobacillus kaustophilus HTA426. Microbiology (Reading) 158:1942-1952.
883 66. Yoshida KI, Shibayama T, Aoyama D, Fujita Y. 1999. Interaction of a repressor and its binding
884 sites for regulation of the Bacillus subtilis iol divergon. J Mol Biol 285:917-29.
885 67. Berman T, Magasanik B. 1966. The pathway of myo-inositol degradation in Aerobacter
886 aerogenes. Ring scission. J Biol Chem 241:807-13.
887 68. Boutte CC, Srinivasan BS, Flannick JA, Novak AF, Martens AT, Batzoglou S, Viollier PH, Crosson S.
888 2008. Genetic and computational identification of a conserved bacterial metabolic module. PLoS
889 Genet 4:e1000310.
890 69. Kröger C, Fuchs TM. 2009. Characterization of the myo-inositol utilization island of Salmonella
891 enterica serovar Typhimurium. J Bacteriol 191:545-54.
892 70. Kröger C, Stolz J, Fuchs TM. 2010. myo-Inositol transport by Salmonella enterica serovar
893 Typhimurium. Microbiology (Reading) 156:128-138.

894 71. Fry J, Wood M, Poole PS. 2001. Investigation of myo-inositol catabolism in Rhizobium
895 leguminosarum bv. viciae and its effect on nodulation competitiveness. Mol Plant Microbe
896 Interact 14:1016-25.
897 72. Gauchat-Feiss D, Frey J, Belet M, Deshusses J. 1985. Cloning of genes involved in myo-inositol
898 transport in a Pseudomonas sp. J Bacteriol 162:324-7.
899 73. Legakis NJ, Papavassiliou JT, Xilinas ME. 1976. Inositol as a selective substrate for the growth of
900 Klebsiellae and Serratiae. Zentralbl Bakteriol Orig A 235:453-8.
901 74. Primrose SB, Ronson CW. 1980. Polyol metabolism by Rhizobium trifolii. J Bacteriol 141:1109-14.
902 75. Reber G, Belet M, Deshusses J. 1980. Energetics of myo-inositol transport in Pseudomonas
903 putida. Experientia 36:528-9.
904 76. Krings E, Krumbach K, Bathe B, Kelle R, Wendisch VF, Sahm H, Eggeling L. 2006. Characterization
905 of myo-inositol utilization by Corynebacterium glutamicum: the stimulon, identification of
906 transporters, and influence on L-lysine formation. J Bacteriol 188:8054-61.
907 77. Hellinckx J, Fuchs TM. 2017. Hysteresis in myo-inositol utilization by Salmonella Typhimurium.
908 Microbiologyopen 6(2):e00431.
909 78. Müller J, Spriewald S, Stecher B, Stadler E, Fuchs TM. 2019. Evolutionary Stability of Salmonella
910 Competition with the Gut Microbiota: How the Environment Fosters Heterogeneity in
911 Exploitative and Interference Competition. J Mol Biol 431:4732-4748.
912 79. Herrou J, Crosson S. 2013. myo-inositol and D-ribose ligand discrimination in an ABC periplasmic
913 binding protein. J Bacteriol 195:2379-88.
914 80. Elston RA, Hasegawa H, Humphrey KL, Polyak IK, Häse CC. 2008. Re-emergence of Vibrio
915 tubiashii in bivalve shellfish aquaculture: severity, environmental drivers, geographic extent and
916 management. Dis Aquat Organ 82:119-34.
917 81. Kehlet-Delgado H, Richards GP, Häse C, Mueller RS. 2017. Three Draft Genome Sequences of
918 Vibrio coralliilyticus Strains Isolated from Bivalve Hatcheries. Genome Announc 5(41):e01162-
919 17.
920 82. Tang K, Zhan W, Zhou Y, Xu T, Chen X, Wang W, Zeng Z, Wang Y, Wang X. 2020. Antagonism
921 between coral pathogen Vibrio coralliilyticus and other bacteria in the gastric cavity of
922 scleractinian coral Galaxea fascicularis. Science China Earth Sciences 63:157-166.
923 83. Drew D, North RA, Nagarathinam K, Tanabe M. 2021. Structures and General Transport
924 Mechanisms by the Major Facilitator Superfamily (MFS). Chem Rev 121:5289-5335.
925 84. Thompson JD, Higgins DG, Gibson TJ. 1994. CLUSTAL W: improving the sensitivity of progressive
926 multiple sequence alignment through sequence weighting, position-specific gap penalties and
927 weight matrix choice. Nucleic Acids Res 22:4673-80.
928 85. Jones DT, Taylor WR, Thornton JM. 1992. The rapid generation of mutation data matrices from
929 protein sequences. Comput Appl Biosci 8:275-82.
930 86. Ohbayashi T, Cossard R, Lextrait G, Hosokawa T, Lesieur V, Takeshita K, Tago K, Mergaert P,
931 Kikuchi Y. 2022. Intercontinental Diversity of Caballeronia Gut Symbionts in the Conifer Pest Bug
932 Leptoglossus occidentalis. Microbes Environ 37(3):ME22042.
933 87. Shu L, Zhang B, Queller DC, Strassmann JE. 2018. Burkholderia bacteria use chemotaxis to find
934 social amoeba Dictyostelium discoideum hosts. Isme j 12:1977-1993.
935 88. Kaltenpoth M, Flórez LV. 2020. Versatile and Dynamic Symbioses Between Insects and
936 Burkholderia Bacteria. Annu Rev Entomol 65:145-170.
937 89. Acuña-Rodríguez IS, Newsham KK, Gundel PE, Torres-Díaz C, Molina-Montenegro MA. 2020.
938 Functional roles of microbial symbionts in plant cold tolerance. Ecol Lett 23:1034-1048.
939 90. Tran C. 2022. Coral-microbe interactions: their importance to reef function and survival. Emerg
940 Top Life Sci 6:33-44.

941 91. Sweet M, Villela H, Keller-Costa T, Costa R, Romano S, Bourne DG, Cárdenas A, Huggett MJ,
942 Kerwin AH, Kuek F, Medina M, Meyer JL, Müller M, Pollock FJ, Rappé MS, Sere M, Sharp KH,
943 Voolstra CR, Zaccardi N, Ziegler M, Peixoto R. 2021. Insights into the Cultured Bacterial Fraction
944 of Corals. mSystems 6:e0124920.
945 92. Gregory GJ, Boas KE, Boyd EF. 2020. The organosulfur compound dimethylsulfoniopropionate
946 (DMSP) is utilized as an osmoprotectant by Vibrio species. Appl Environ Microbiol 87(5):e02235-
947 20.
948 93. Gregory GJ, Dutta A, Parashar V, Boyd EF. 2020. Investigations of Dimethylglycine, Glycine
949 Betaine, and Ectoine Uptake by a Betaine-Carnitine-Choline Transporter Family Transporter with
950 Diverse Substrate Specificity in Vibrio Species. J Bacteriol 202:e00314-20.
951 94. Naughton LM, Blumerman SL, Carlberg M, Boyd EF. 2009. Osmoadaptation among Vibrio species
952 and unique genomic features and physiological responses of Vibrio parahaemolyticus. Appl
953 Environ Microbiol 75:2802-10.
954 95. Ongagna-Yhombi SY, Boyd EF. 2013. Biosynthesis of the osmoprotectant ectoine, but not glycine
955 betaine, is critical for survival of osmotically stressed Vibrio parahaemolyticus cells. Appl Environ
956 Microbiol 79:5038-49.
957 96. Martins LO, Carreto LS, Da Costa MS, Santos H. 1996. New compatible solutes related to Di-myo-
958 inositol-phosphate in members of the order Thermotogales. J Bacteriol 178:5644-51.
959 97. Empadinhas N, Mendes V, Simões C, Santos MS, Mingote A, Lamosa P, Santos H, Costa MS.
960 2007. Organic solutes in Rubrobacter xylanophilus: the first example of di-myo-inositol-
961 phosphate in a thermophile. Extremophiles 11:667-73.
962 98. Lamosa P, Rodrigues MV, Gonçalves LG, Carr J, Ventura R, Maycock C, Raven ND, Santos H.
963 2013. Organic solutes in the deepest phylogenetic branches of the Bacteria: identification of
964 α(1-6)glucosyl-α(1-2)glucosylglycerate in Persephonella marina. Extremophiles 17:137-46.
965 99. Rodrigues MV, Borges N, Almeida CP, Lamosa P, Santos H. 2009. A unique beta-1,2-
966 mannosyltransferase of Thermotoga maritima that uses di-myo-inositol phosphate as the
967 mannosyl acceptor. J Bacteriol 191:6105-15.
968 100. Galbraith MP, Feng SF, Borneman J, Triplett EW, de Bruijn FJ, Rossbachl S. 1998. A functional
969 myo-inositol catabolism pathway is essential for rhizopine utilization by Sinorhizobium meliloti.
970 Microbiology (Reading) 144 (Pt 10):2915-2924.
971 101. Janda JM, Abbott SL, McIver CJ. 2016. Plesiomonas shigelloides Revisited. Clin Microbiol Rev
972 29:349-74.
973 102. Xu T, Rasmussen-Ivey CR, Moen FS, Fernández-Bravo A, Lamy B, Beaz-Hidalgo R, Khan CD, Castro
974 Escarpulli G, Yasin ISM, Figueras MJ, Azzam-Sayuti M, Karim MM, Alam KMM, Le TTT, Thao NHP,
975 Addo S, Duodu S, Ali S, Latif T, Mey S, Somony T, Liles MR. 2023. A Global Survey of
976 Hypervirulent Aeromonas hydrophila (vAh) Identified vAh Strains in the Lower Mekong River
977 Basin and Diverse Opportunistic Pathogens from Farmed Fish and Other Environmental Sources.
978 Microbiol Spectr 11:e0370522.
979 103. Hossain MJ, Waldbieser GC, Sun D, Capps NK, Hemstreet WB, Carlisle K, Griffin MJ, Khoo L,
980 Goodwin AE, Sonstegard TS, Schroeder S, Hayden K, Newton JC, Terhune JS, Liles MR. 2013.
981 Implication of lateral genetic transfer in the emergence of Aeromonas hydrophila isolates of
982 epidemic outbreaks in channel catfish. PLoS One 8:e80943.
983 104. Rasmussen-Ivey CR, Hossain MJ, Odom SE, Terhune JS, Hemstreet WG, Shoemaker CA, Zhang D,
984 Xu DH, Griffin MJ, Liu YJ, Figueras MJ, Santos SR, Newton JC, Liles MR. 2016. Classification of a
985 Hypervirulent Aeromonas hydrophila Pathotype Responsible for Epidemic Outbreaks in Warm-
986 Water Fishes. Front Microbiol 7:1615.
987 105. Davin-Regli A, Lavigne JP, Pagès JM. 2019. Enterobacter spp.: Update on Taxonomy, Clinical
988 Aspects, and Emerging Antimicrobial Resistance. Clin Microbiol Rev 32(4):e00002-19.

989 106. Ma B, Hibbing ME, Kim HS, Reedy RM, Yedidia I, Breuer J, Glasner JD, Perna NT, Kelman A,
990 Charkowski AO. 2007. Host range and molecular phylogenies of the soft rot enterobacterial
991 genera pectobacterium and dickeya. Phytopathology 97:1150-63.
992 107. Charkowski AO. 2018. The Changing Face of Bacterial Soft-Rot Diseases. Annu Rev Phytopathol
993 56:269-288.
994 108. O'Banion BS, Jones P, Demetros AA, Kelley BR, Knoor LH, Wagner AS, Chen JG, Muchero W,
995 Reynolds TB, Jacobson D, Lebeis SL. 2023. Plant myo-inositol transport influences bacterial
996 colonization phenotypes. Curr Biol 33:3111-3124.e5.
997 109. Sánchez-Gil JJ, Poppeliers SWM, Vacheron J, Zhang H, Odijk B, Keel C, de Jonge R. 2023. The
998 conserved iol gene cluster in Pseudomonas is involved in rhizosphere competence. Curr Biol
999 33:3097-3110.e6.
1000 110. Matthews JL, Khalil A, Siboni N, Bougoure J, Guagliardo P, Kuzhiumparambil U, DeMaere M, Le
1001 Reun NM, Seymour JR, Suggett DJ, Raina JB. 2023. Coral endosymbiont growth is enhanced by
1002 metabolic interactions with bacteria. Nat Commun 14:6864.
1003 111. T DA, Krause L, Bridge T, Torda G, Raina JB, Zakrzewski M, Gates RD, Padilla-Gamiño JL, Spalding
1004 HL, Smith C, Woolsey ES, Bourne DG, Bongaerts P, Hoegh-Guldberg O, Leggat W. 2015. The coral
1005 core microbiome identifies rare bacterial taxa as ubiquitous endosymbionts. Isme j 9:2261-74.
1006 112. Dehio C, Meyer M. 1997. Maintenance of broad-host-range incompatibility group P and group Q
1007 plasmids and transposition of Tn5 in Bartonella henselae following conjugal plasmid transfer
1008 from Escherichia coli. J Bacteriol 179:538-40.
1009 113. Pederson K, Verdonck L, Austin B, Austin D, Blanch AR, Grimont PAD, Jofre J, Koblavi S, Larsen JL,
1010 Tianinen T, Vigneulle M, Swings J. 1998. Taxonomic evidence that Vibrio carchariae Grimes et al.
1011 1985 is a junior synonym of Vibrio harveyi (Johnson and Shunk 1936) Baumann et al. 1981.
1012 International Journal of Systematic and Evolutionary Microbiology 48:748-749.
1013 114. Gregory GJ, Morreale DP, Carpenter MR, Kalburge SS, Boyd EF. 2019. Quorum Sensing
1014 Regulators AphA and OpaR Control Expression of the Operon Responsible for Biosynthesis of the
1015 Compatible Solute Ectoine. Appl Environ Microbiol 85(22):e01543-19.
1016 115. Gibson DG. 2011. Enzymatic assembly of overlapping DNA fragments. Methods Enzymol
1017 498:349-61.
1018 116. Philippe N, Alcaraz JP, Coursange E, Geiselmann J, Schneider D. 2004. Improvement of pCVD442,
1019 a suicide plasmid for gene allele exchange in bacteria. Plasmid 51:246-55.
1020 117. Kumar S, Stecher G, Li M, Knyaz C, Tamura K. 2018. MEGA X: Molecular Evolutionary Genetics
1021 Analysis across Computing Platforms. Mol Biol Evol 35:1547-1549.
1022 118. Saitou N, Nei M. 1987. The neighbor-joining method: a new method for reconstructing
1023 phylogenetic trees. Mol Biol Evol 4:406-25.
1024 119. Robert X, Gouet P. 2014. Deciphering key features in protein structures with the new ENDscript
1025 server. Nucleic Acids Res 42:W320-4.
1026 120. Jumper J, Evans R, Pritzel A, Green T, Figurnov M, Ronneberger O, Tunyasuvunakool K, Bates R,
1027 Žídek A, Potapenko A, Bridgland A, Meyer C, Kohl SAA, Ballard AJ, Cowie A, Romera-Paredes B,
1028 Nikolov S, Jain R, Adler J, Back T, Petersen S, Reiman D, Clancy E, Zielinski M, Steinegger M,
1029 Pacholska M, Berghammer T, Bodenstein S, Silver D, Vinyals O, Senior AW, Kavukcuoglu K, Kohli
1030 P, Hassabis D. 2021. Highly accurate protein structure prediction with AlphaFold. Nature
1031 596:583-589.
1032 121. Hastings J, Owen G, Dekker A, Ennis M, Kale N, Muthukrishnan V, Turner S, Swainston N,
1033 Mendes P, Steinbeck C. 2016. ChEBI in 2016: Improved services and an expanding collection of
1034 metabolites. Nucleic Acids Res 44:D1214-9.

1035 122. Murail S, de Vries SJ, Rey J, Moroy G, Tufféry P. 2021. SeamDock: An Interactive and
1036 Collaborative Online Docking Resource to Assist Small Compound Molecular Docking. Front Mol
1037 Biosci 8:716466.
1038 123. Felsenstein J. 1985. CONFIDENCE LIMITS ON PHYLOGENIES: AN APPROACH USING THE
1039 BOOTSTRAP. Evolution 39:783-791.

1040

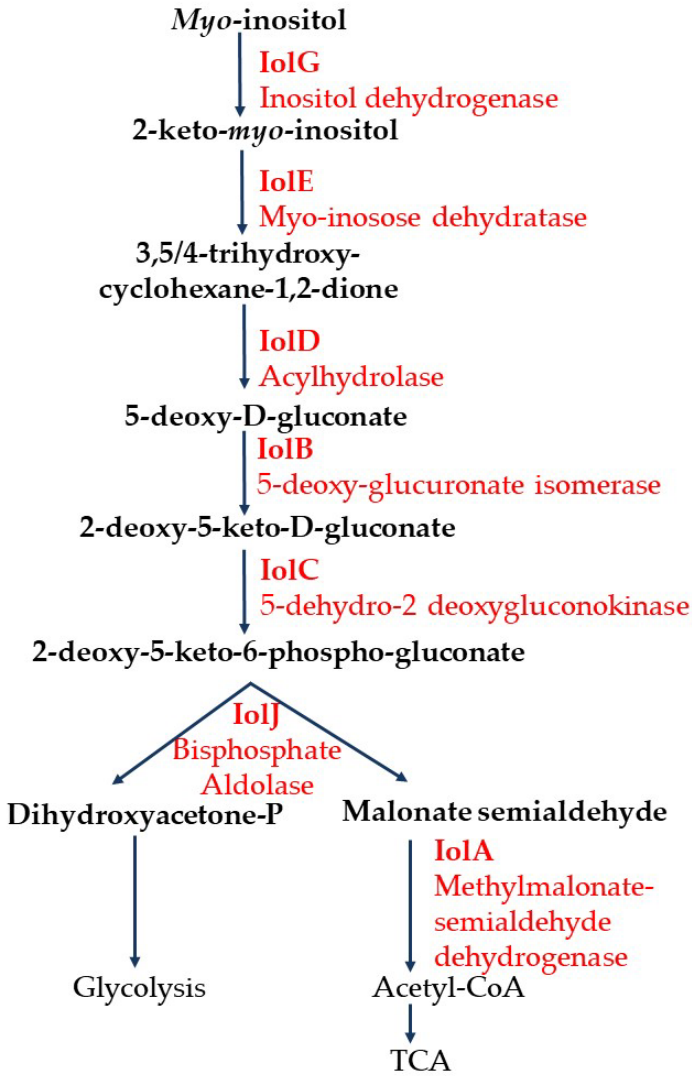

Fig. 1. Pathway of m*yo*-inositol catabolism. The pathway presented is based upon studies in *B. subtilis* and *Salmonellla enterica*. Enzymes (red) and intermediate compounds in the pathway are displayed.

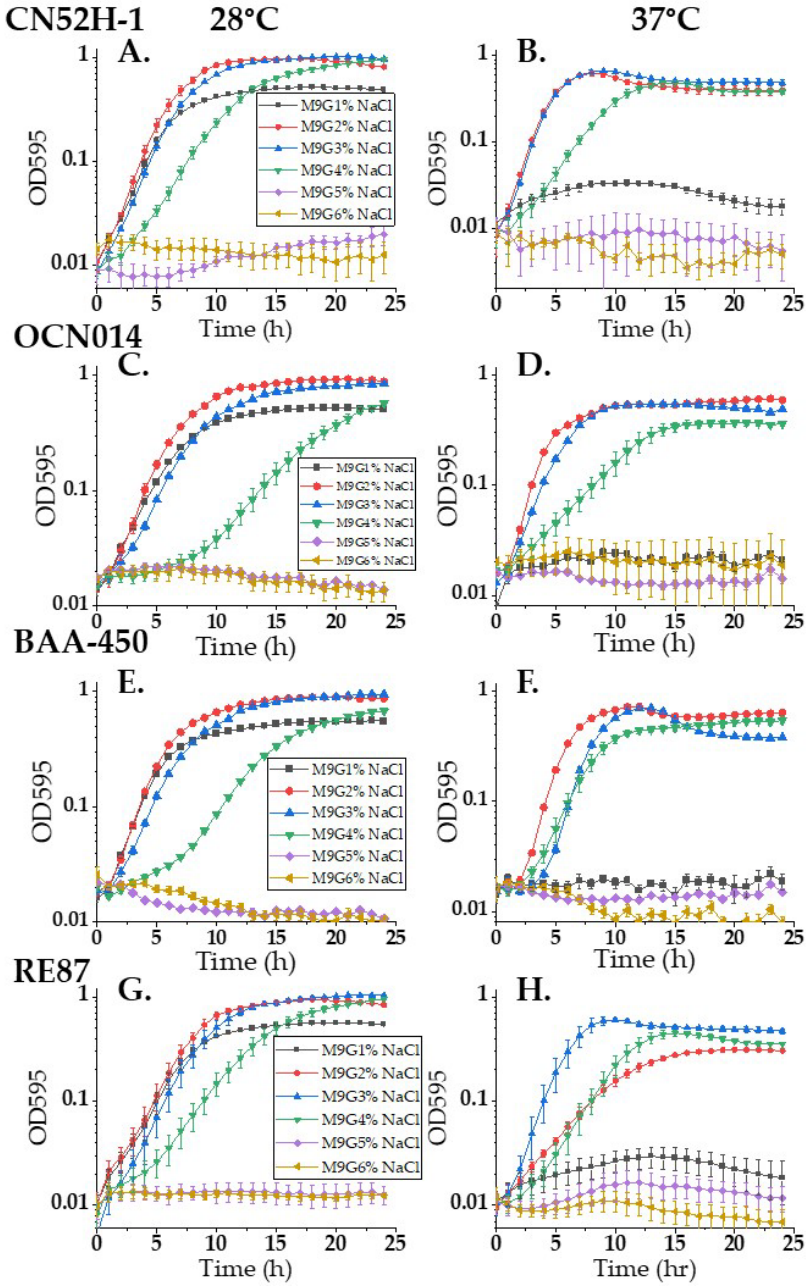

Fig. 2. *Vibrio coralliilyticus* NaCl tolerance range. Growth curves of *V. coralliilyticus* strains in minimal media (M9) with glucose (M9G) with a final concentration of 1% to 6% NaCl. Growth was measured every hour for 24 h at **A.** 28°C strain CN52H-1, **B.** 37°C strain CN52H-1, **C.** 28°C strain OCN014, **D.** 37°C strain OCN014, **E.** 28°C strain BAA-450, **F.** 37°C strain BAA-450, **G.** 28°C strain RE-87, **H.** 37°C strain RE-87 . Mean and standard deviation of three biological replicates are shown.

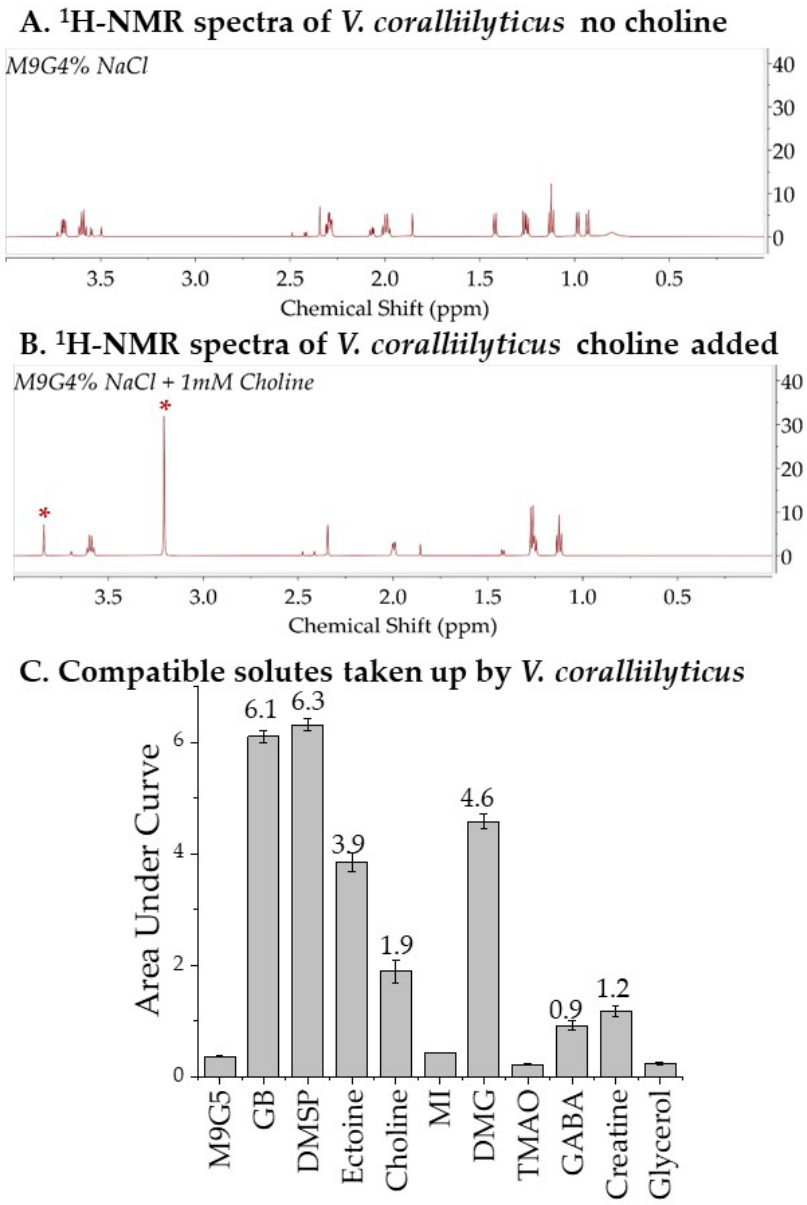

Fig. 3. ***V. coralliilyticus*** **compatible solute biosynthesis and uptake systems. A.** ¹H-NMR spectra of *V. coralliilyticus* CN52H-1 cellular extract grown in minimal media (M9G) 4% NaCl without choline and **B.** with the addition of 1 mM choline. The spectral peaks corresponding to glycine betaine are labeled with red asterisks. **C.** *V. coralliilyticus* was inoculated into M9G 5% NaCl with 1 mM GB (glycine betaine), DMSP (dimethylsulfoniopropionate), ectoine, choline, MI (*myo*-inositol), DMG (dimethylglycine), trimethylamine N-oxide (TMAO), gamma-aminobutyric acid (GABA), creatine, or glycerol. Growth was measured for 24 h at 28°C and the calculated area under the curve AUC calculated shown above each compatible solute that rescued growth. Mean and standard deviation of three biological replicates are shown.

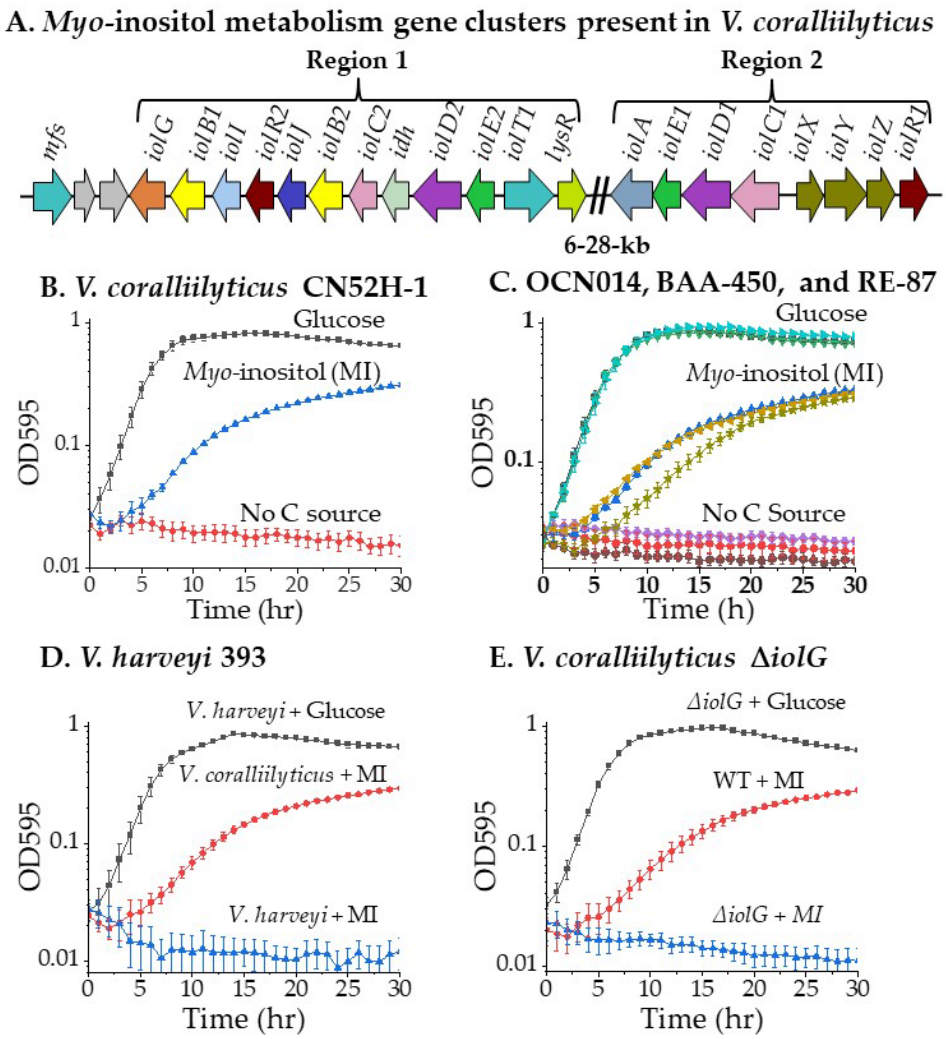

Fig. 4. *V. coralliilyticus* utilized *myo*-inositol as a sole carbon source. A. Schematic of the gene order of *myo*-inositol transporter, catabolism and regulatory genes in *V. coralliilyticus*. **B.** Growth curve analysis in minimal media (M9 2% NaCl) containing either 20 mM glucose (squares) or 20 mM *myo*-inositol (MI, triangles) or no carbon source (circles) for *V. coralliilyticus* CN52H-1. **C.** *V. coralliilyticus* strains OCN014, BAA-450, and RE-87. **D.** *V. harveyi* 393 and **E.** *V. coralliilyticus* Δ*iolG.* Growth was measured every hour for 30 h at 28°C. Mean and standard deviation of four biological replicates are shown.

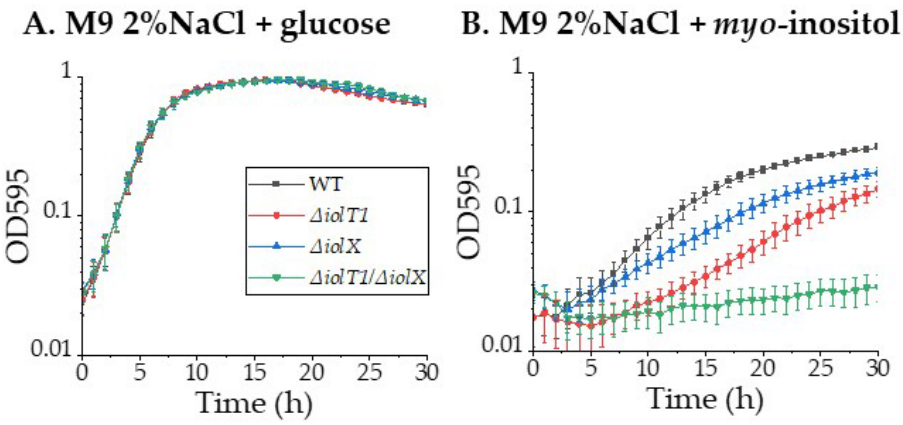

Fig. 5. Growth pattern analysis of *V. coralliilyticus myo*-inositol transporters deletion mutants. Growth analysis of wild type, Δ*iolT1*, Δ*iolX*, and Δ*iolT1*/ Δ*iolX* in minimal media (M9 2% NaCl) with **A.** 20 mM glucose or **B.** 20 mM *myo*-inositol as a sole carbon source. Growth was measured every hour for 30 h at 28°C. Mean and standard deviation of three biological replicates are shown.

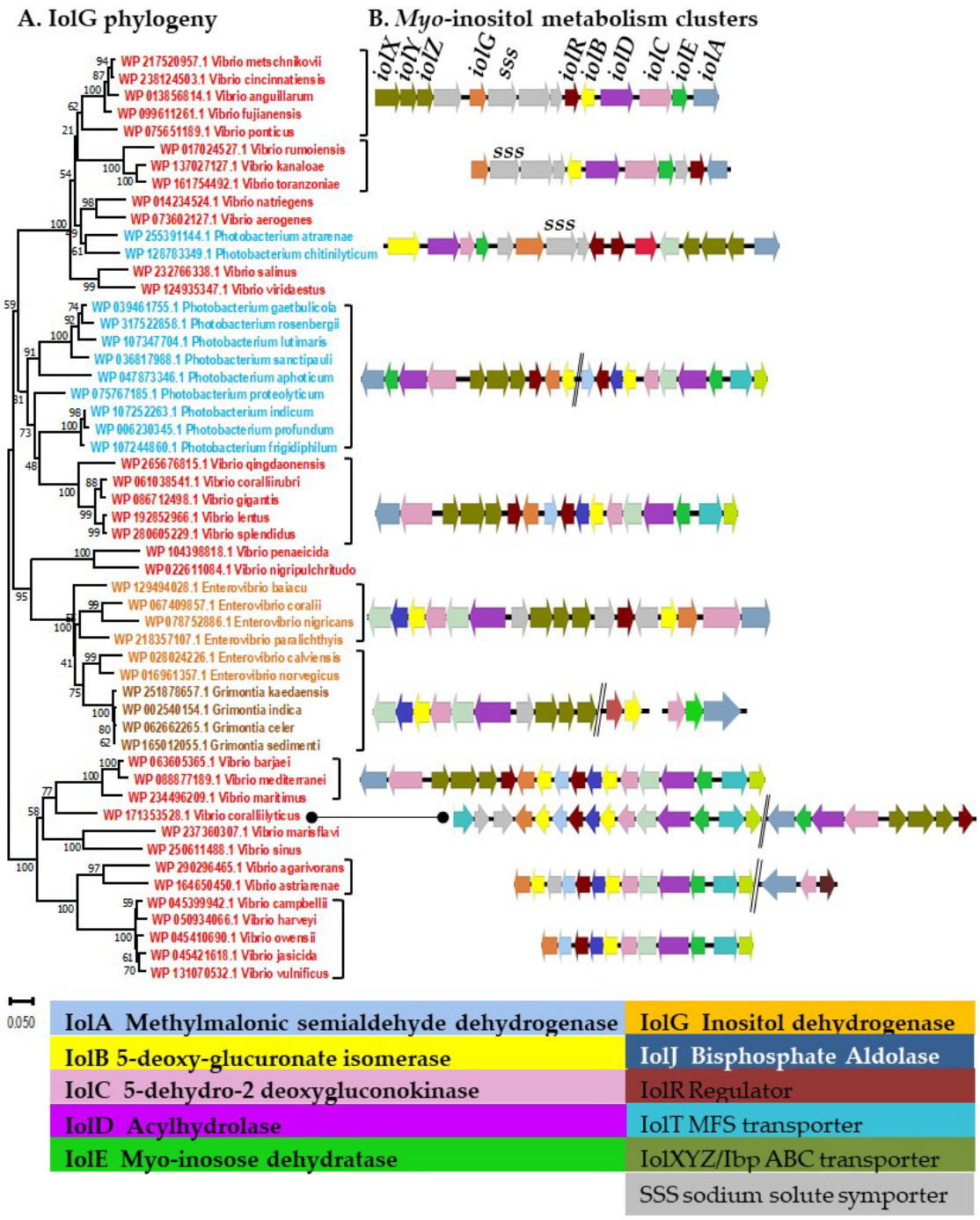

Fig. 6. Phylogenetic distribution of IolG and Iol cluster organization among *Vibrionaceae*. A. IolG evolutionary history was inferred using the Neighbor-Joining method (118) with bootstrap value of 1000 (123). The optimal tree with the sum of branch length = 4.11930205 is shown. The tree is drawn to scale, and evolutionary distances were computed using the JTT matrix-based method (85) with units of the number of amino acid substitutions per site. Shown are 53 amino acid sequences, ambiguous positions were removed for each sequence pair (pairwise deletion option) with a total of 332 positions. Evolutionary analyses were conducted in MEGA X (117). IolG was present in only 32 *Vibrio* (red), 11 *Photobacterium* (blue), 6 *Enterovibrio* (orange), and 4 *Grimontia* (brown) species. **B**. Iol cluster organization among *Vibrionaceae* species. Arrows represent open reading frame and direction of transcription, double black lines represent genes between regions.

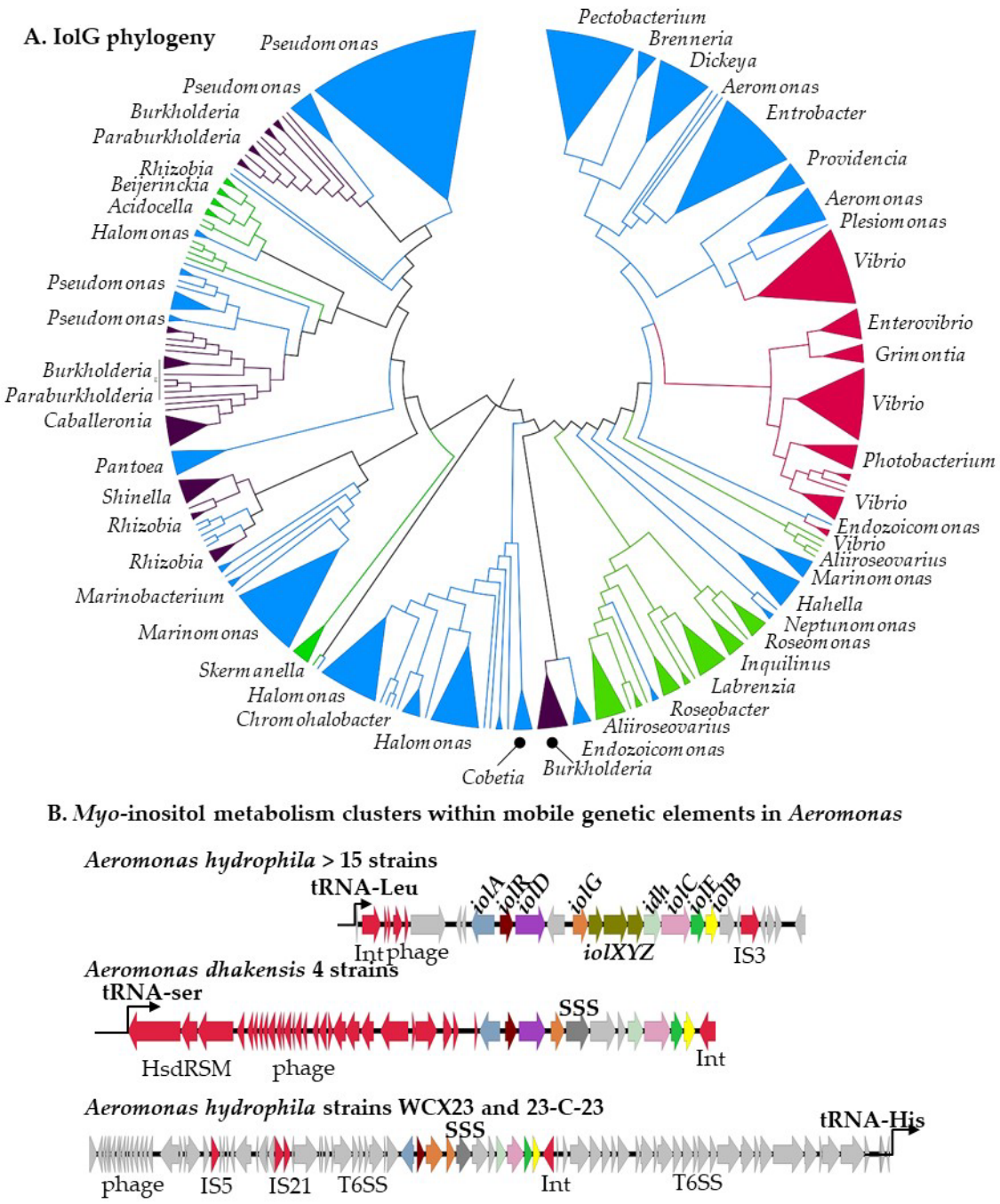

Fig. 7. IolG phylogeny among marine species. Condensed consensus tree with collapsed branches is shown, original tree is shown in **Fig. S11**. IolG phylogeny was inferred using the Neighbor-Joining method (118). This analysis involved 358 amino acid sequences. Blue and red collapsed branches represent Gamma-, purple represents Beta-, and green represents Alpha-Proteobacteria. **B.** Genome context of *myo*-inositol metabolism clusters within mobile genetic elements in *Aeromonas* species.